

Selection of the fittest or selection of the luckiest: the emergence of Goodhart’s law in evolution

Bastien Mallein^{*}, Francesco Paparella[†], Emmanuel Schertzer[‡], Zsófia Talyigás[§]

March 31, 2025

Abstract

Biological evolution depends on the passing down to subsequent generations of genetic information encoding beneficial traits, and on the removal of unfit individuals by a selection mechanism. However, selection acts on phenotypes, and is affected by random contingencies. Thus, a combination of fitness and luck determines which individuals will successfully reproduce and give rise to the next generation. To understand how randomness in the selection mechanism affects the long-term patterns of evolution, we studied an idealized evolution model. We show through simulations and mathematical analysis, that the speed of adaptation increases with increasing selection pressure only up to a threshold. Beyond the threshold, any increase of the selection pressure results in more weight given to random effects rather than on genetic fitness in determining which individuals will successfully reproduce. This severely reduces the speed of adaptation and the diversity in the gene pool. Our findings may be considered as a biological instance of Goodhart’s law: “When a measure becomes a target, it ceases to be a good measure”. Finally, we show that this intricate response of evolution to natural selection can be mathematically explained by a novel phase transition for pulled traveling waves.

1 Introduction

In the classical book “The Genetical Theory of Natural Selection” [21] mathematical population geneticist Fisher begins by stating that “natural selection is not evolution.” Natural selection operates within a generation and favors certain phenotypes over others. In contrast, evolution by natural selection involves the transmission of these favored phenotypes to the next generation, which requires that the advantageous traits are at least partially heritable [37]. Thus, for selection to operate over time, the fitness advantage provided by a specific trait must have a genetic basis that can be transmitted to the next generation. Trait transmission and selection are then two distinct mechanisms and both are necessary in order for Darwinian evolution to exist. Ever since Fisher, much work has been devoted to understanding the consequences of the aleatory nature of trait transmission, particularly when sexual reproduction is at play. However, selection operates through specific and contingent interactions of individual phenotypes with the environment in which they live, and it is completely oblivious of the underlying genotype. Thus, although selection ultimately determines which genotypes are preserved and transmitted and which are weeded out, we have to recognize that selection, too, is a noisy, aleatory process.

In order to fully understand long-term, large-scale patterns of evolution, we believe that it is crucial to consider the evolutionary effects of noisy selection schemes. Because the selection criterion that occurs in any given situation is a noisy version of that which would be optimal for improving the genes that determine the traits subject to selective pressure, we should be careful in assuming that optimal

^{*}Institut de Mathématiques de Toulouse, UMR 5219, Université de Toulouse, UPS, F-31062 Toulouse Cedex 9, France

[†]Division of Science and Mubadala Arabian Center for Climate and Environmental Science. New York University Abu Dhabi, Saadiyat Island, Abu Dhabi, United Arab Emirates

[‡]Faculty of Mathematics, University of Vienna, Oskar-Morgenstern-Platz 1, 1090 Wien, Austria

[§]Faculty of Mathematics, University of Vienna, Oskar-Morgenstern-Platz 1, 1090 Wien, Austria

improvement of those traits will be the necessary outcome of evolution. The misalignment between the optimal selection criterion and the actual, noisy one is not free of consequences. Understanding the side effects of repeatedly using an optimization criterion in place of another (which may be impossible to implement) while aiming at achieving the same end goal, is emerging as a very important problem in the fields of evolutionary algorithms and artificial intelligence [28, 32, 39], as well as in the context of academic selection procedures [35]. In economics, the fact that the use of observed statistics (phenotype) for regulatory purposes (selection process) eventually fails to achieve the intended goal is called Goodhart’s law [24, 15]. In this paper, we argue that similar failures must occur in biological evolutionary processes.

We consider an idealized stochastic population model in which each individual possesses a *genotype*, identified as a real number, representing the genotypic fitness of the individual. The genotype consists in the inherited information transmitted from parent to children. The expression of that genotype is called *phenotype*. In Biology, the genotype to phenotype map may be influenced by extrinsic and intrinsic noises such as developmental noise [23], phenotypic heterogeneity [4], cellular noise [30], biological noise [18] and intra-genotypic variability [5]. Finally, we will prescribe that selection acts on phenotypic values but that only the genotypic information propagates from one generation to the next. Our approach will rely on the observation that the population can be approximated over large time scale as a discrete fitness wave [27] describing the steady state of the population at a constant speed. We will leverage this approach to demonstrate how phenotypic noise and selection strength can drastically influence the response to selection.

Rate of adaptation. We will first demonstrate that there exists a critical threshold for selective pressure delineating a *strong* and a *weak* selection regime. In the weak selection regime, the rate of adaptation increases with selective pressure until that threshold is reached but slows down if the selective pressure exceeds the threshold. We will also demonstrate that selection operates differently in these two regimes. In the strong regime, selection pressure results in more weight given to random effects rather than on genetic fitness in determining which individuals will successfully reproduce (*selection of the luckiest*), at the expense of the fittest individuals. In the weak selection regime, however, despite the inherent randomness of the selection process, a fraction of the fittest individuals is consistently preserved (*selection of the fittest*).

Genetic variation. In the absence of selection, all individuals in a population have the same expected number of descendants, and fluctuations of neutral alleles in the population are the by-product of random sampling alone. When selection favors certain individuals, those individuals contribute more offspring to the next generation, skewing the distribution of reproductive success and reducing the number of individuals contributing to the next generation. Thus, selection can significantly reduce genetic variation within a population and impair the adaptive capacity of the population, increasing the risk of extinction under changing conditions. As a consequence, the rate of adaptation is arguably a narrow measure of the response to selection and it is also of fundamental importance to understand the impact of selection and noise on neutral genetic variation, as measured here by the effective population size [12]. We will see that beyond its detrimental impact on the rate of adaptation, an excessive selection pressure also leads to a sharp decline in genetic variation during the transition from the weak to the strong regime.

2 The model

We first consider an asexual population subject to viability selection, i.e., selection only acts at the age of reproduction and provides a selective advantage to individuals with the highest phenotypes. We assume a discrete time dynamic consisting of $K \gg 1$ individuals and where the population evolves according to two sub-steps.

Reproduction. Each individual produces a fixed number of offspring r . These children inherit the genotype of their parent up to an independent random fluctuation owed to the occurrence of random mutations. The phenotype is determined by a random fluctuation of the genotypes. More precisely, the child of an individual with genotype g has genotype $g + X$ and phenotype

$g + X + Y$ where (X, Y) is a pair of independent random variables with prescribed densities f_X and f_Y (see later).

Selection. Following reproduction, the population consists of rK individuals. To regulate the size of the population, the K individuals with the largest *phenotypes* survive and give birth to the next generation, transmitting their *genotypes*. As a consequence, selection acts according to phenotypes, but only genetic information is propagated to the next generation.

The variable $N = Kr$ represents the total number of individuals after reproduction and will be interpreted as the carrying capacity of the population. Another variable of interest is

$$\gamma := \log(K)/\log(N) = \log(K)/\log(rK)$$

so that the fertility of a single individual during the reproduction phase is approximately $N^{1-\gamma}$, whereas $K = N^\gamma$ is the number of individuals passing their genes to the next generation so that γ encodes the fraction of the population allowed to reproduce in a log scale (*reproduction skewness*). For a fixed value of carrying capacity N , a lower γ entails a higher selection pressure since only a reduced number N^γ of individuals can reproduce; whereas a high γ (close to 1) corresponds to a mild selection scheme where almost every children survive to the next generation. As a consequence, γ can be interpreted as capturing the selection pressure in the population. When γ is low, the selection pressure is strong; when γ is high, the selection pressure is weak. Throughout our numerical and mathematical analysis, we will assume that N is large but that γ remains fixed. This entails that the fertility $r = N^{1-\gamma}$ of individuals before selection is typically large.

We now make some assumptions on the genetic noise distribution f_X , and the phenotype noise distribution f_Y . For the sake of simplicity, we assume that both phenotypic and genotypic noises have super-exponential tails. Let $\alpha \geq 1$ and $\mu, \lambda > 0$ such that

$$f_X(x) = C_{\lambda,\alpha} \exp(-(\lambda|x|)^\alpha), \quad f_Y(x) = C_{\mu,\alpha} \exp(-(\mu|x|)^\alpha),$$

with $C_{\cdot,\cdot}$ being positive normalization constants. The case $\alpha = 1$ corresponds to the Laplace distribution, $\alpha = 2$ to the Gaussian distribution. Up to a change of unit of measure, one can assume without loss of generality that $\lambda = 1$ so that μ now represents the ratio of the genotypic standard deviation (std) vs the phenotypic std.

3 Transition from the weak to the strong selection regimes

We first exposed numerical simulations, taking interest in the rate of adaptation and the effective population size of this population model for different levels of phenotypic noise μ and selection pressure γ (see Figure 1).

Rate of adaptation. We observe that the rate of adaptation is not monotone as a function of the selection pressure, and we define $\gamma_c(\mu)$ as the value of the selection pressure that maximizes the rate of adaptation for a given value of the phenotypic noise (black line in Figure 3). The function $\mu \mapsto \gamma_c(\mu)$ segregates the parameters (μ, γ) of our models into two domains, that correspond to two regimes for the branching-selection process. We will from now on say that a pair of parameters such that $\gamma < \gamma_c(\mu)$ is in the *strong selection regime*, whereas $\gamma > \gamma_c(\mu)$ is the *weak selection regime*. Indeed, let us recall that a higher γ entails that more adults are allowed to reproduce in the next generation, so that a higher selection pressure translates into a lower γ .

In the weak selection regime ($\gamma > \gamma_c(\mu)$), increasing the selection pressure (i.e. decreasing γ) has the effect of increasing the rate of adaptation, as the set of parents that will be able to reproduce to the next generation will be fitter on average. In the strong selection regime ($\gamma < \gamma_c(\mu)$), this effect is counter-intuitively reversed: increasing the selection pressure has the effect of *decreasing* the rate of adaptation of the population.

As a result, a selection pressure of $\gamma_c(\mu)$ entails a maximal rate of adaptation for the population. The selection pressure is too weak in the weak regime to optimize the speed of adaptation, whereas it is

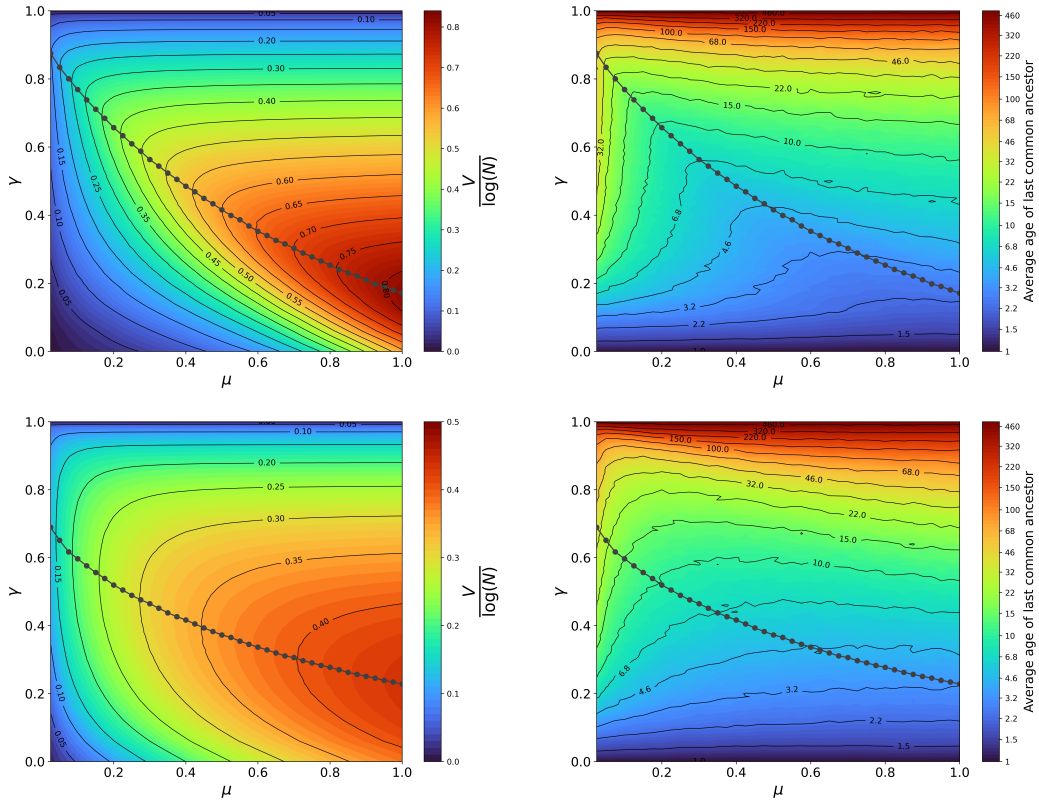


Figure 1: Rates adaptations and effective population sizes in a branching-selection particle system with a population of size 10^5 , plotted as a function of the genotypic to phenotypic standard deviation ratio μ and the selection pressure γ . The *Top Panels* were simulated using $\alpha = 1$ (Laplace distribution for the phenotypic and genotypic distributions), whereas the *Bottom Panels* were made using $\alpha = 2$ (Gaussian distribution for phenotypic and genotypic distributions). The phenomenological picture appears identical for different values of $\alpha \geq 1$. *Left Panels*: Estimated rate of adaptation of the genotype profile. The dotted line corresponds to the critical line $\gamma_c(\mu)$ segregating the strong and the weak regime (respectively lower and upper part of the figure). For each μ , $\gamma_c(\mu)$ is the selection pressure that maximises the rate of adaptation. *Right Panels*: The effective population size N_e . The same function $\mu \mapsto \gamma_c(\mu)$ computed from the corresponding left panel is reproduced.

too strong in the strong selection regime and has a detrimental effect on the evolution of the population. This latter case corresponds to an instance of Goodhart's law, i.e., the *objective* (maximisation of the genotypic value) is impaired by overfitting the *measure* (phenotypic values). The mathematical treatment of this model will allow us to reveal a clear explanation behind this phenomenon.

Effective population size. Our numerical simulations reveal a second evolutionary signature of the transition from the weak to the strong regime, evident in the neutral genetic variation within the population.

Neutral genetic variation is assessed through ancestral properties of the population [16]. By sampling two individuals in the present and tracing their ancestral lineages backward in time, we can determine the most recent common ancestor (MRCA), with its distance to the present denoted as T_2 . Under the molecular clock hypothesis [16], the number of observed neutral segregating mutations is predicted to be proportional to $\mathbb{E}(T_2)$, linking genetic diversity to the depth of the population's genealogical structure. To quantify genetic variation, we then use the effective population size [12], defined as $N_e = \mathbb{E}(T_2)$, as shown in the right panels of Fig. 1.

Our first observation is that the effective population size is significantly lower in the strong regime, indicating a strong loss of genetic diversity in the strong regime. Secondly, a fundamental question

in population genetics is understanding how natural selection influences neutral genetic diversity [21]. Since the field's inception [20, 25, 26, 45], it has been widely believed that stronger directional selection leads to a reduction in genetic diversity. However, our simulations reveal a counterintuitive phenomenon. In our model, reducing noise enhances the one-step effectiveness of selection by aligning the phenotype and genotype of each individual more closely. Based on traditional intuition, this should lead to reduced genetic diversity. Yet, our findings suggest that the relationship between phenotypic noise (μ) and the response to selection is non-monotonic, with genetic diversity reaching its minimum approximately along the critical line separating the two regimes (see again Figure 3). Notably, in the weak regime, we observe the surprising effect that reduced noise (decreasing μ) increases the effective population size. In other words, intensifying selection by lowering noise also increases the effective population size in the weak regime.

4 Deterministic evolution and ancestral structures

Our numerical simulations suggest the existence of a critical line at which the key evolutionary parameters of the model (rate of adaptation and effective population size) exhibit a non-monotone response to the selection parameters (selection pressure (γ) and phenotypic noise (μ)). To explain the observed transition, we now turn to the mathematical analysis of the model, in which we focus on the Laplace case ($\alpha = 1$) which is particularly amenable to analysis.

4.1 Log-profiles.

Numerical simulations (see top left panel of Fig. 2) reveal that genotypes and phenotypes are typically highly concentrated around the mean of the population. Moreover, the distribution of genotypes in the population, on a logarithmic scale, appears to quickly stabilize on a profile, that travels as a wave over time. We take interest in the dynamic of this logarithmic profile, which describes the extreme genotypes in the population (carried by N^a individuals for some $a < \gamma$). The typical highest increment of the genotype in a generation being $O(\log(N))$, we rescale this profile appropriately.

More precisely, we define the genotypic profile g of a population as a quantity valued in $\mathbb{R}_+ \cup \{-\infty\}$ so that the number of particles around $x \log(N)$ is approximately given by $N^{g(x)}$. In other words, $g(x)$ can be thought of as the limiting stochastic exponent of the population in N . In PDE, this is often referred to as the Hopf-Cole transformation of the system (see e.g. [11]). Note that when $g(x) = -\infty$, this corresponds to having no particle present around x . We also consider the phenotypic profile $p(x)$ so that $N^{p(x)}$ captures the number of phenotypes *to the right* of $x \log(N)$ after the reproduction step.

Let (X, Y) be a pair of independent random variables with Laplace distributions of parameter 1 and μ respectively. Direct computations yield that

$$\begin{aligned} \log \mathbb{P}(X + Y > y \log N) &\approx -\min(\mu, 1)y_+ \log N \\ \text{and } \log \mathbb{P}(X \approx x \log N, X + Y > y \log N) &\approx -(|x| + \mu(y - x)_+) \log N \end{aligned} \quad (4.1)$$

where we write $x_+ = \max(x, 0)$. Writing g_n for the genotypic profile of a population at the n th generation, and p_n for the phenotypic profile of its children, we observe that (g_n, p_n) evolve according to the following deterministic dynamics

$$\begin{aligned} p_n(x) &= \pi \left[1 - \gamma + \sup_{y \in \mathbb{R}} (g_{n-1}(y) - \min(1, \mu)(x - y)_+) \right] \\ s_n &= \sup\{x \in \mathbb{R} : p_n(x) \geq \gamma\} \\ g_n(x) &= \pi \left[1 - \gamma + \sup_{y \in \mathbb{R}} (g_{n-1}(y) - |x - y| - \mu(s_n - x)_+) \right], \end{aligned} \quad (4.2)$$

with

$$\pi(x) = \begin{cases} x & \text{if } x \geq 0 \\ -\infty & \text{if } x < 0 \end{cases}$$

Let us provide a quick justification for those formulas based on the tail estimates (4.1). The $N^{g_{n-1}(y)}$ individuals with genotype approximately $y \log N$ at generation $n - 1$ will create on average

$$N^{g_{n-1}(y)+1-\gamma-\min(1,\mu)(x-y)_+}$$

phenotypes larger than $x \log N$ at generation n . As a consequence, the number of phenotypes larger than x is given by the above formula after integrating over y and using the Laplace method –which can be detected in the sup of the first equation. The projector π expresses that if the average number of individuals around $y \log N$ goes to 0 as $N \rightarrow \infty$ then the probability of observing such an individual also becomes vanishingly small.

The value s_n is then computed such that there are around N^γ individuals with phenotype larger than $s_n \log N$. Finally, we obtain $g_n(x)$ by estimating (in the same manner) the number of children with genotype around $x \log N$ and phenotype larger than $s_n \log N$. The function π has the effect of only conserving the positive part of g_n as if $g_{n-1}(x) - |y - x| - \mu(s_n - y)_+ + 1 - \gamma < 0$, then with high probability none of the individuals at position $x \log N$ will have a descendant at position $y \log N$ with a phenotype larger than $s_n \log N$.

We show in SM (Proposition S.2.4) that the evolution can be rephrased in terms of a discrete “free-boundary” problem

$$g_n(x) = \pi \left[1 - \gamma + \sup_{y \in \mathbb{R}} (g_{n-1}(y) - |x - y| - \mu(s_n - y)_+) \right], \quad (4.3)$$

where s_n satisfies $\sup g_n = \gamma$,

where the second condition reflects the fact that the phenotypic threshold s_n can solely be determined by the condition that there are N^γ individuals left after enforcing the selection step.

4.2 Traveling wave solution

We only take interest in the long-term asymptotic behaviour of the profile (g_n) defined by (4.2). We say that a function g is a traveling wave for the dynamic (4.2) with speed v if, assuming that $g_0 = g$, we have

$$g_n(x) = g(x - nv). \quad (4.4)$$

In other words, the dynamic has the effect of shifting the genotypic profile by v , where v is interpreted as the speed of evolution in the natural scale of the system ($\log(N)$ for $\alpha = 1$; $\sqrt{\log(N)}$ for $\alpha = 2$ as in the numerical simulations of Fig. 1). Examples of such traveling wave solutions, and convergence to those, are depicted in Fig. 2.

In SM, we show the existence and uniqueness of a traveling wave solution under minimal assumptions (Theorem S.1.1). The crucial part of this result is the existence of a transition segregating the parameter space (μ, γ) into two sub-regions delimited by an explicit curve

$$\gamma_c : \mu \mapsto \gamma_c(\mu) := \frac{\lfloor 1/\mu \rfloor}{\lfloor 1/\mu \rfloor + 1} \left(1 - \frac{\mu}{2 - \lfloor 1/\mu \rfloor \mu} \right), \quad (4.5)$$

drawn in the bottom left panel of Fig. 3 (in solid black), and corresponding to distinct evolutionary regimes mirroring our numerical simulations. The regime $\gamma < \gamma_c(\mu)$ will correspond to the strong regime, whereas the case $\gamma > \gamma_c(\mu)$ corresponds to the weak regime. Our deterministic analysis allows us to first characterize the phase transition in 2 different ways which reflect the numerical observations of Fig. 1.

Fully and semi pulled waves. First, the critical curve $\gamma_c(\mu)$ delineates a phase transition between semi and fully waves which is new to our knowledge. As we shall see, this transition reflects the loss of genetic diversity in the strong regime.

To explain the nature of the transition, we first note that the dynamics of the wave contains some partial information on the ancestral structure of the underlying population. Recall that

$$g_n(x) = \pi \left[1 - \gamma + \sup_{y \in \mathbb{R}} (g_{n-1}(y) - |x - y| - \mu(s_n - x)_+) \right].$$

where the maximization problem arises from integrating the contribution of all the population at time $n - 1$ and then applying the Laplace method to extract the main contribution at x from the previous generation. This overwhelming contribution by a single location is captured by the sup in the previous formula. This entails that the ancestor of an individual at position x is likely to be found at positive

$$\text{Argmax}_{y \in \mathbb{R}} (g_{n-1}(y) - |x - y| - \mu(s_n - x)_+)$$

in the previous generation. Let us now consider an individual at distance x from the extremal genotypes (right tip of the wave). From the previous equation, we deduce that the distance of its ancestor from the tip (of the wave in the previous generation) is given by

$$A(x) = \text{Argmax}_{y \in \mathbb{R}} \{g(y) - |x + v - y|\}, \quad (4.6)$$

where g is the traveling wave. Let $A^{(n)}$ be the n th iteration of the ancestral map A . In turn, the genotype of the ancestor n generations backward in time is at distance $A^{(n)}(x)$ from the tip of the wave n generations backward in time. It turns out that the two evolutionary regimes dictate different behaviors for the ancestral map A . This is formally proved in Theorem S.1.2 in SM, and graphically explained in the bottom panels of Fig 2.

In the strong regime, $A^{(n)}(x)$ reaches 0 in finitely many generations so that the ancestor of any individual is directly at the tip of the wave. Thus, the wave at a given time is generated (or pulled) by few extremal individuals close to the tip and is said to be *fully-pulled*. See bottom right panel of Fig 2.

For the weak regime, $A^{(n)}(x)$ also reaches an equilibrium in finitely many generations. However, and in contrast to the strong regime, the maximization problem (4.6) becomes degenerate. More precisely, iterating the ancestral map A gets the ancestor closer to 0 (i.e. closer to the tip). After a few iterations, the maximum of the ancestral function A is not attained at a single point but on an interval that we refer to as the *ancestral interval*. See bottom left panel of Fig 2. The interpretation of this phenomenon is that the positions of ancestors of an individual is uniformly distributed on the ancestral interval after a few generations. A crucial observation is that the ancestral interval (1) contains the tip, but (2) does not contain the bulk, that is, the point where the wave is maximized. As a consequence of (2), ancestral individuals deviate substantially from the mean but in contrast to the strong regime, a typical ancestor is not directly at the tip, but instead it is uniformly distributed on the ancestral interval. Thus, the wave is still pulled by extremal individuals, but those extremal individuals are typically located at an intermediary location between the tip and the mean. The wave is now said to be only *semi-pulled*.

This shift in the ancestral properties of the traveling wave suggests a loss of genetic diversity in the strong regime in accordance with the right panels of Fig. 1. In the strong regime, our previous analysis indicates that the population at time t originates from only the very few individuals at the tip of the wave as indicated by the fact that $A^{(n)} = 0$ after a few backward generations. In contrast, in the weak regime, the population traces back to a broader set of ancestors captured by the ancestral interval, and whose size scales as $\log(N)$ in the original scale. These observations will be further refined in Section 4.3.

Selection of the fittest or selection of the luckiest. Secondly, our mathematical results (Theorem S.1.1. in SM) identify the phase transition observed in numerical simulations for the rate of adaptation in accordance to the left panels of Fig. 1. Below the critical curve ($\gamma < \gamma_c(\mu)$ strong regime/fully pulled), lowering selection by increasing γ has the effect of increasing the rate of adaptation. Above the critical curve (weak selection/semi-pulled, $\gamma > \gamma_c(\mu)$) the effect is reversed so that the optimal level of selection is attained at the intermediary level $\gamma_c(\mu)$.

Our analysis reveals a clear explanation behind this phenomenon. Consider the population right after reproduction (that is before implementing the selection step). There are $N = rK$ genotypes available among which $K < N$ will be chosen according to their phenotypes in the selection phase. We now ask the following question: since selection only acts on phenotypes, do we always pick the very best genotype? The answer depends on the evolutionary regime at hand.

- *The strong/fully-pulled regime entails selection of the luckiest:* the best genotype is never picked;
- *The weak/semi-pulled regime entails selection of the fittest:* the best genotype is always selected.

To give an intuition behind this phenomenon, we note that when selection is strong ($\gamma < \gamma_c$), we only allow for a few individuals to reproduce. This is obviously a risky strategy since selection only picks a few individuals whose phenotype can potentially inflate their underlying genotypes. In contrast, the weak regime enforces a diversification of the risk so that the highest genotype is always picked. In other words, the extremes of the phenotypic and genotypic spaces are partially decorrelated, and when selection is too strong, it will miss the children with exceptionally high genotype.

Beyond the intuition, the previous statement is made mathematically precise in Theorem S.1.3 and the preceding paragraphs in SM. The content of this formal result is related to geometric properties of the traveling wave solution as illustrated in Figure 2. Essentially, the distinction between the strong and the weak regime can be seen in the position of the phenotypic threshold s . Recall that s corresponds to the minimal phenotypic value in order to be selected at the next generation. We assume that the population has reached the traveling wave state and we start from a population with a genotypic makeup corresponding to the traveling wave (blue) at time t , and make one step of the evolution to obtain the profile at time $t + 1$ (4.2) (green). This genotypic profile is constructed in two successive steps: we first generate the genotypic profile of the children (orange), and then obtain the genotypic at $t + 1$ (green) profile by thinning the profile with our selection procedure. In particular, the difference between the orange and the green curve corresponds to the log-number of genotypes eliminated during the selection process. We can now distinguish between two geometries of the wave.

In the strong selection regime, the threshold s exceeds the reproduction profile (orange) indicating that surviving individuals must have an exceptionally high phenotypes to reach the phenotypic threshold s . As it is apparent from the figure, the tip of the reproduction curve (orange) is strictly higher than the genotypic curve at time $t + 1$ (blue) indicating that all the children with the best genotypes are washed out by selection. (All the children located between the two tips are not selected.) Therefore, in the strong selection regime, the survival of each individual is partially explained by having an unusually high phenotype. As the (few) individuals with a very high genotype will tend to have average phenotype, those are therefore not preserved by the selection step, which explains the drop in the rate of adaptation of the population.

In contrast, in the weak selection regime, all the children with a genotype above s will be selected. Geometrically, this corresponds to the alignment of the reproduction curve (orange) and the curve at time 1 (green) curves.

Low phenotypic noise. If $\mu > 1$, a close inspection of Eq. (4.5) reveals that $\gamma_c(\mu) = 0$ so that only the strong regime persists. In this regime, the large increment of the phenotype of an individual is primarily explained by a large increment of its genotype (see Eq. 4.1), and no non-trivial optimum may be found for the selection pressure (γ) when we optimise on the rate of adaptation (v). That is, in this case, we have $\gamma_c = 0$, meaning that the optimal adaptation rate is to select a constant (independent of N) number of individuals with the largest phenotypes.

4.3 Effective population size

The right panels of Fig. 1 indicates (i) a loss of genetic diversity in the strong regime, and (ii) that the genealogical structure of the population exhibits a non-monotone response to a change of the phenotypic noise (μ). Further, the change of monotonicity occurs exactly at the critical curve segregating the weak and the strong selection regime. We now provide a mathematical explanation for this intriguing phenomenon.

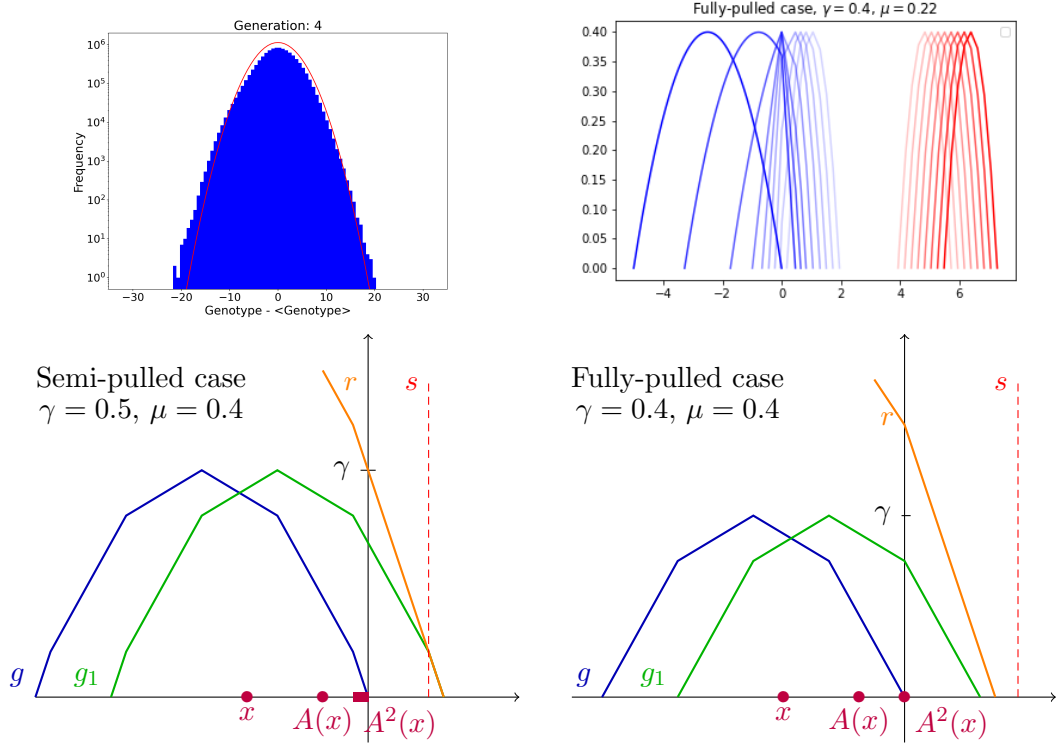


Figure 2: *Top left panel.* Distribution of genotypes in a large population, plotted on a logarithmic scale. We observe for large populations the apparition of a deterministic genotypic profile. The profile is well approximated by a quadratic profile (in red). *Top right panel.* Convergence to the traveling wave solution of the deterministic dynamic, started from an initial Gaussian distribution (i.e. a parabolic log-profile). Blue curves show the evolution of the first 8 steps of the genotypic profile, the red curves steps 16 to 24. We observe that by that time, the phenotypic profile has converged to a traveling wave solution. *Bottom panels.* Schematic description of the iteration of the traveling wave over one step. The blue line represents the initial traveling wave profile, the orange line the genotypic profile of the children (that is after reproduction). The green line correspond to the genotypic profile of the selected children, and is a translation of the blue profile. The vertical red dotted line corresponds to the position of the selection threshold –in particular, note that the green and orange lines are identical to the right of that threshold, indicating that genotypes to the right of the threshold will be selected. The bottom purple dots correspond to iterations of the ancestral function in the stationary setting indicating the successive ancestors in the population.

The effective population size is defined as the expected coalescence time of two distinct ancestral lineages. While our earlier analysis is based on deterministic approximations, the genealogical structure of the system retains its stochastic nature in the large population limit and random coalescence times cannot be inferred solely from the hydrodynamic limit. Consequently, the genealogical structure of the population (and thus N_e) highly depends on the system fluctuations.

Analyzing system fluctuations is inherently more complex, so we address this challenge using a proxy model inspired by the exponential branching random walk (BRW) developed by Brunet, Derrida, and collaborators [7, 9]. In this original model, individuals reproduce an infinite number of offspring distributed according to an exponential Poisson point process centered on the parental value. After reproduction, truncation selection is applied, retaining only the K rightmost genotypes. This framework was originally introduced to provide the first analytical approach to studying fluctuations in F-KPP fronts, leveraging the particle system’s integrability.

A recent generalization, known as the noisy exponential BRW, modifies this framework by blurring the effect of selection: offspring are reproduced as before but instead of truncation selection, individuals are randomly selected according to Gibbs sampling [14, 44]. For more details, see Section S.4.2 of the SM.

Although the noisy exponential BRW may initially seem distinct from our study, Section S.4.2 of the SM will demonstrate that the differences are largely superficial. We show that the noisy BRW retains many key features of the original model, including a similar hydrodynamic limit and the transition between semi-pulled and fully pulled regimes. This suggests that both models belong to the same universality class and share similar genealogical structures. By leveraging the integrability of the noisy BRW and results derived in [44], we compute the effective population size for this integrable model. Comparing universal quantities between the two models allows us to propose an ansatz for the effective population size in the original model.

$$\forall \gamma < \gamma_c(\mu), \quad N_e(\mu, \gamma) \approx \frac{1}{\mu} \quad (4.7)$$

$$\forall \gamma > \gamma_c(\mu), \quad N_e(\mu, \gamma) \approx \chi(\mu, \gamma) \log(N). \quad (4.8)$$

where $\chi(\mu, \gamma)$ is the size of the ancestral interval and is given by Eq. (S.3.8) in Theorem S.3.1 in SM and is in good qualitative accordance with our numerical simulations. See Fig 3. We note that the discontinuity in the theoretical predictions corresponds to a first order phase transition and that this discontinuity is smoothed out in the finite population regime.

Our mathematical results provide an explanation for two phenomena observed in numerical simulations. First, the effective population size is lower in the strong regime ($N_e = O(1)$) as compared to the weak regime ($N_e = O(\log(N))$). Secondly, $\mu \rightarrow N_e(\mu, \gamma)$ is non monotone, and as in Fig 1, the change of monotonicity again occurs at the critical line.

Finally, our comparative approach allows to extract more information on the ancestral structure of the population. Whereas N_e only depends on the coalescence time of two lineages, our comparative analysis allows to describe the random genealogy spanned by any number of lineages. In SM, we show that in the weak regime (resp. strong regime) the genealogy should converge to a Bolthausen-Sznitman coalescent (resp., Poisson Dirichlet coalescent) [41]. See Section S.4.2 for more details.

4.4 Convergence to the deterministic limit.

Rate of convergence. Figure 3 demonstrates that our deterministic approximations offer a reliable qualitative prediction of the stochastic model. Notably, the finite-size particle system retains a similar phenomenological structure to its deterministic counterpart, including the sharp phase transition between the *weak selection* and *strong selection* regimes, as shown in Figure 3. However, the convergence to the hydrodynamic limit is observed to occur at an exceptionally slow rate.

This slow convergence is a well-documented characteristic of branching-selection particle systems [8]. To better understand the deviations from the infinite population limit, we utilize the noisy BRW introduced in Section S.4.2 and compute the convergence rate in SM, Section S.4.2. The speed of convergence of the adaptation rate occurs at a very slow $(\log N)^{-1}$ rate. More precisely, writing $v_{\mu, \gamma}$ the rate of adaptation of the deterministic model, and $v_{\mu, \gamma}^{(N)}$ the rate of adaptation of the finite size

model with N^γ individuals selected at each generation, we have

$$\frac{v_{\mu,\gamma}^{(N)}}{\log(N)} - v_{\mu,\gamma} \sim \begin{cases} \frac{\Xi(\mu,\gamma)}{\log N} & \text{if } \gamma < \gamma_c \\ \frac{\log(\Xi(\mu,\gamma) \log N)}{\log N} & \text{if } \gamma > \gamma_c \end{cases}$$

See top right panel of Figure 3. Note that the speed of convergence is consistent with the one observed in the original model. See top left panel of Figure 3.

Corrections to the limiting profile. The predictions of quantitative genetics models rely on the simplifying assumptions that the genotypes distributions remain Gaussian along time (see [42] and the references therein) – or equivalently that log-profiles are quadratic. In contrast, starting from our individual based model, the traveling wave solution is a piecewise linear profile in the log-scale, as shown in Theorem S.3.1 in SM and the bottom panels of Fig. 2. This suggests that the cornerstone assumptions of quantitative genetics do not hold under our high fertility scenario. However, as indicated from the previous discussion, higher order corrections play a significant role in finite populations, and our numerical simulations suggest that profiles are still well approximated by a quadratic profile. See top right panel of Fig 2.

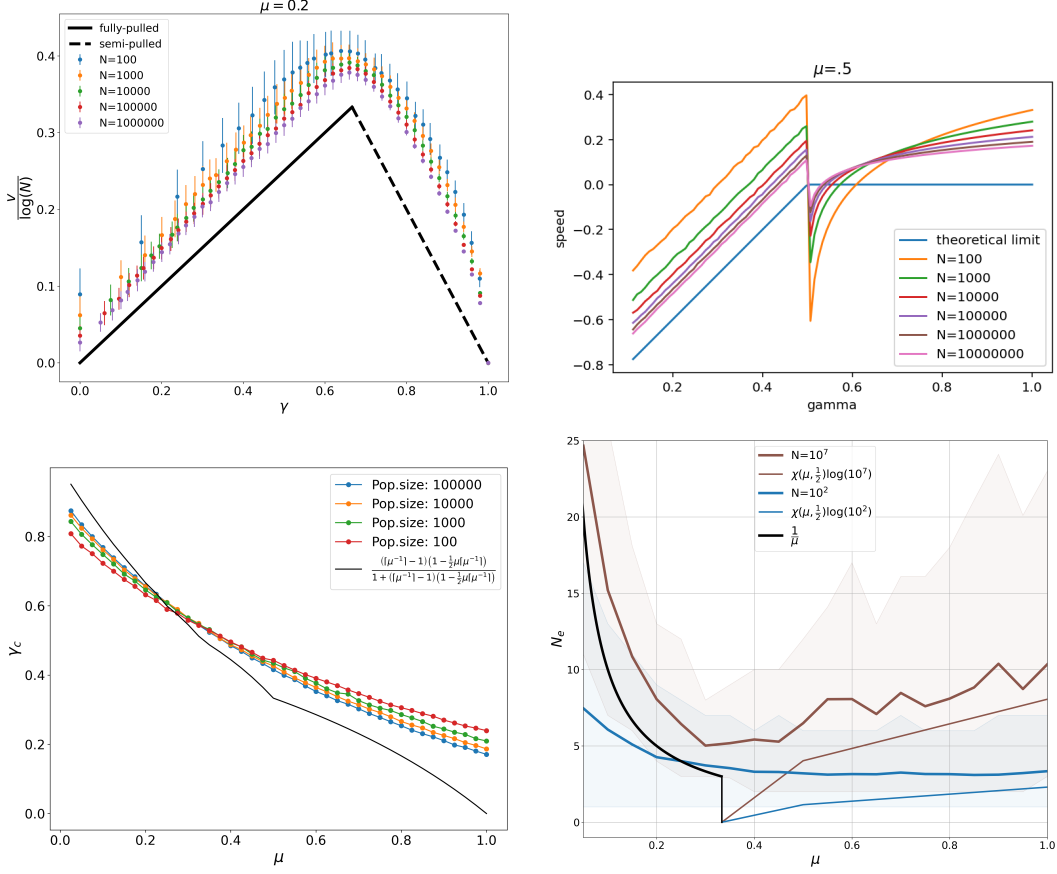


Figure 3: *Top panels.* Rate of adaptation for the deterministic limiting model and its finite-size population correction, for the original stochastic model on the *left panel*, and the noisy BRW *right panel* (believed to be its scaling limit). In both cases, the rate of convergence is notably slow.

Bottom left panel. Comparison between the critical value γ_c estimated for each μ as the value of γ maximizing $\gamma \mapsto v_{\gamma, \mu}^{(N)}$. *Bottom right panel.* Effective population size for $N = 10^7$ (thick brown curve, average over 100 realizations) and $N = 10^2$ (blue curve, average over 1000 realizations). The shaded areas show the 10th to 90th percentiles of the distribution. The solid black line is the theoretical approximation (S.4.7) in the strong regime; the thin brown and blue lines are the theoretical approximation (S.4.8) in the weak selection regime. For large populations ($N = 10^7$), a change of monotonicity occurs close to the closed predicted value which corresponds to the end point of the curve $1/\mu$.

4.5 Sexual reproduction.

In SM (Section S.6), we also present a sexual version of our model. In this version, each of the N children chooses two parents uniformly at random in the population, inherits their average genotype plus a random fluctuation X of law f_X . Once again, the phenotype of a child is obtained by perturbing its genotype by a random fluctuation Y of law f_Y .

Therein, we show that the log-profile of the population evolves according to a modified recursive free boundary problem (4.2) as follows

$$g_n(x) = \pi \left[1 - 2\gamma + \sup_{y \in \mathbb{R}} (2g_{n-1}(y) - |x - y| - \mu(s_n - x)_+) \right], \quad (4.9)$$

where s_n satisfies $\sup g_n = \gamma$.

In particular, note the apparition of a $2g_{n-1}(y)$ corresponding to the selection of two parents. It is interesting to observe that in this deterministic limit, every individual surviving will have two parents with a roughly equal genotypic value.

Even if the recursive equations of the sexual and asexual case look similar at first sight, sexual populations exhibits a much richer behavior and we postpone its mathematical analysis for future work.

First, a similar transitions when $\mu \in [1/2, 1]$, that is when the the phenotypic noise is at intermediary value. In this case, Figure 4 shows that the speed of evolution is also maximized at intermediary values of $\gamma_c(\mu)$. However, our simulations show a complex critical line with some resonance-like modes. In addition, we exhibit a regime which was not present in the asexual case. When the phenotypic noise is too high ($\mu < \frac{1}{2}$), the speed of evolution stabilizes to 0 indicating that the population remains static on the natural space scaling of the system (measured in $\log(N)$ units). See Figures 4,5. Finally, our models predicts that the speed of evolution is always higher in the asexual case.

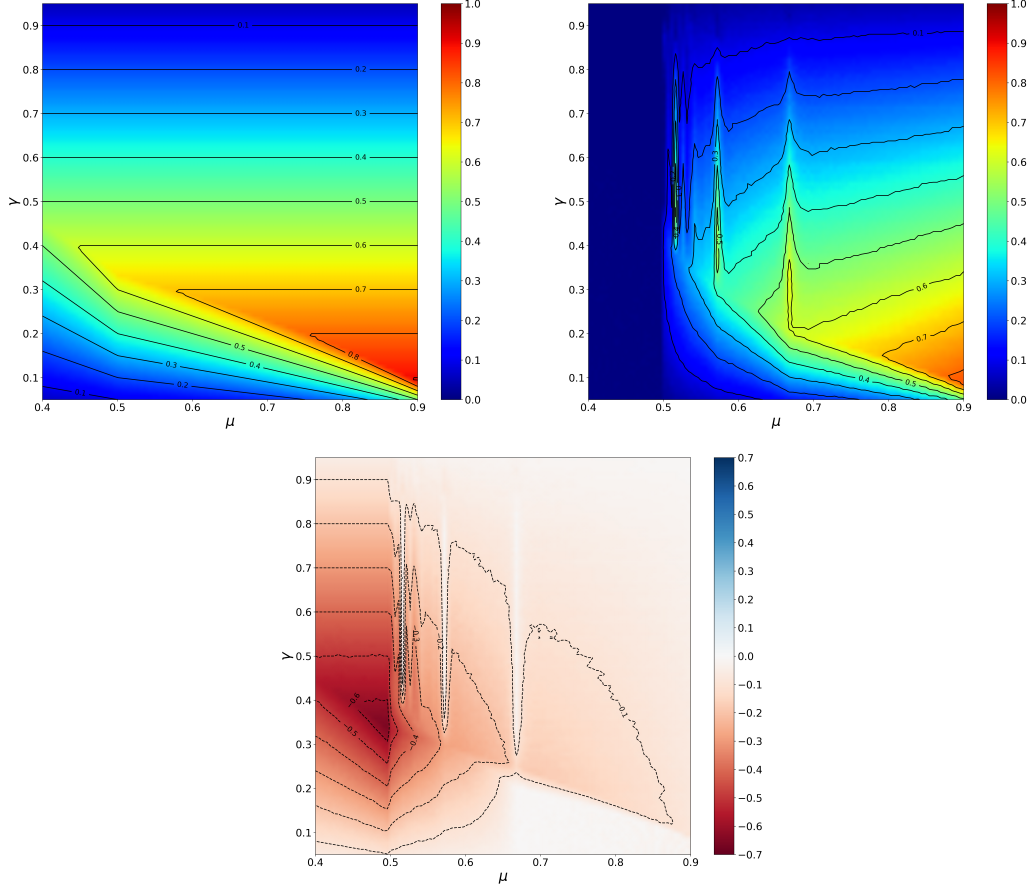


Figure 4: *Left panel.* Speed for the asexual model as predicted by the explicit solution of (4.3). *Right panel.* Speed for the sexual model as predicted by the iterating the modified equation (4.9). For both models, if $\mu \in (.5, 1)$, the speed is maximized at intermediary values. However, in the sexual case, the speed is always 0 when the phenotypic noise is too large $\mu < 1/2$. *Bottom panel.* Comparison of the speed of evolution in the sexual and asexual models.

5 Discussion

Understanding the response to selection is at the heart of population genetics. To highlight the novelty of the present approach, we first would like to highlight how the present paper differs from some classic approaches. As a concrete example, Lande [36] considered a similar problem in the context of quantitative genetics, [19]. He considered a population represented as a Gaussian cloud of points, with selection acting on a correlated phenotypic traits. Assuming that the original genotype distribution and phenotypic noise are Gaussian, Lande provided a mathematical description of the response to selection in a single generation. In contrast, the aim of the present article was to understand the interplay between natural selection and evolution. This requires capturing the effects of selection over a large number generations as the result of selection and mutation. In Lande's work, the response to selection

highly depends on the initial state of the population (standing variation) and the realized heritability of the trait. In contrast, capturing the rate of evolution and genetic drift over evolutionary time scales requires to understand how those imposed parameters emerge from the evolutionary dynamics as a response to natural selection. A key challenge of our work was to derive the genetic composition of a population at "stationarity" (traveling front), where stationarity emerges from the action of natural selection on large evolutionary time scales. In accordance with most of models in quantitative genetics, our numerical simulations suggest that populations are also well approximated by a Gaussian profile (quadratic log-profile as can be seen from the top left panel of Figure 2). However, the population variance is not an imposed parameter, but instead, it emerges as a response to the long-time effect of a noisy selection inducing a complex interplay between natural selection and evolution.

In accordance with the Fisher's quote that "natural selection is not evolution", our model predicts a non linear response of evolutionary parameters (adaptation rate and effective population size) to the selection parameters (selection pressure, phenotypic noise). We identify two main evolutionary regimes –strong and weak – translating into traveling waves of different nature and whose geometry drastically impacts the effect of selection as summarized in the lower panels of Figure 2. When selection is amplified by reducing the number of individuals allowed to reproduce, the system exhibits a Goodhart's effect. When selection is too strong (strong regime), the rate of selection responds negatively to stronger selection and the fittest offspring is never selected (*selection of the luckiest*). In the weak regime, the effect is reversed so that the optimal rate of selection is found at the critical selection strength which segregates between the two regimes. In this case, the highest genotype is always selected (*selection of the fittest*). As a consequence, with enough phenotypic noise ($\mu < 1$), selection can neither be too strong nor too weak for an optimal rate of adaptation.

Recent experimental studies suggest that phenotypic noise could be evolvable [31, 47, 33, 17, 29, 40]. Our model predicts that lowering the noise always improves the rate of adaptation. However, it predicts a non-monotone response to phenotypic noise. In particular, lowering the noise (increasing μ) induces a lower effective population size in the strong regime. This entails that that the evolutionary dynamics in this regime is subject to a trade-off between speed and diversity. Increasing the rate of adaptation comes at a cost of reducing genetic diversity. In contrast, in the weak regime (low noise), genetic diversity and rate of adaption both react positively to noise reduction and the population should evolve as to minimize phenotypic noise.

Finally, our findings uncover a new phase transition for *pulled* waves [6, 2]. This transition resonates with recent findings in the context of the noisy F-KKP equation with Allee effect [3, 46, 43, 22] where the density of individuals is described through the equation

$$\partial_t u = \frac{1}{2} \partial_{xx} u + u(1 - u)(1 + Bu) + \frac{1}{N} \sqrt{u} \eta$$

where B is the Allee effect and η is a white space-time noise capturing demographic stochasticity. If the Allee is strong enough ($B > 2$), the traveling wave are *pushed* (in contrast to the pulled waves encountered in our setting), and stochastic effects segregate pushed waves into a semi and a fully regime. For pulled waves (as in the present work), we uncovered a similar phase transition between a fully-pulled and semi-pulled regime. As highlighted before, a single lineage always lies away from the bulk, that is, far from the mean of the fitness wave. In the fully-pulled regime, ancestral lineages always lie within the very few extreme individuals. In the semi-pulled regime, an ancestral lineage at a typical time lies at an intermediary location between the tip and the bulk. If we now consider several ancestral lineages, the ancestral structure should converge to the Bolthausen-Sznitman coalescent where it is known that coalescences occur at the very extreme individual [6, 2]. Thus, in semi pulled waves, ancestral lineages only reach the very extremal individuals upon a coalescence event.

6 Acknowledgments

F.P. gratefully acknowledges support from the NYUAD Research Insitute through projects CG009 and CG002, as well as from the NYUAD HPC center. E.S. gratefully acknowledges support from the FWF project PAT3816823.

References

- [1] J. Bérard and J.-B. Gouéré. “Brunet-Derrida Behavior of Branching-Selection Particle Systems on the Line”. In: *Communications in Mathematical Physics* 298.2 (2010), pp. 323–342. ISSN: 1432-0916. DOI: 10.1007/s00220-010-1067-y. URL: <https://doi.org/10.1007/s00220-010-1067-y>.
- [2] J. Berestycki, N. Berestycki, and J. Schweinsberg. “The genealogy of branching Brownian motion with absorption”. English. In: *Ann. Probab.* 41.2 (2013), pp. 527–618. ISSN: 0091-1798. DOI: 10.1214/11-AOP728.
- [3] G. Birzu, O. Hallatschek, and K. S. Korolev. “Fluctuations uncover a distinct class of traveling waves”. In: *Proceedings of the National Academy of Sciences* 115.16 (2018), E3645–E3654.
- [4] Z. Bódi et al. “Phenotypic heterogeneity promotes adaptive evolution”. In: *PLoS biology* 15.5 (2017), e2000644.
- [5] M. Bruijning et al. “The evolution of variance control”. In: *Trends in ecology & evolution* 35.1 (2020), pp. 22–33.
- [6] É. Brunet and B. Derrida. “Effect of Microscopic Noise on Front Propagation”. In: *Journal of Statistical Physics* 103 (Apr. 2001), pp. 269–282. DOI: 10.1023/A:1004875804376.
- [7] É. Brunet and B. Derrida. “Shift in the velocity of a front due to a cutoff”. In: *Phys. Rev. E* 56 (3 1997), pp. 2597–2604. DOI: 10.1103/PhysRevE.56.2597. URL: <https://link.aps.org/doi/10.1103/PhysRevE.56.2597>.
- [8] É. Brunet, B. Derrida, and D. Simon. “Universal tree structures in directed polymers and models of evolving populations”. In: *Phys. Rev. E* 78 (6 Dec. 2008), p. 061102. DOI: 10.1103/PhysRevE.78.061102. URL: <https://link.aps.org/doi/10.1103/PhysRevE.78.061102>.
- [9] É. Brunet et al. “Effect of selection on ancestry: an exactly soluble case and its phenomenological generalization”. In: *Phys. Rev. E* 76 (4 2007), p. 041104. DOI: 10.1103/PhysRevE.76.041104. URL: <https://link.aps.org/doi/10.1103/PhysRevE.76.041104>.
- [10] É. Brunet et al. “Noisy traveling waves: Effect of selection on genealogies”. In: *Europhys. Lett.* 76.1 (2006), pp. 1–7. DOI: 10.1209/epl/i2006-10224-4. URL: <https://doi.org/10.1209/epl/i2006-10224-4>.
- [11] Nils Caillerie. “Large deviations of a forced velocity-jump process with a Hamilton-Jacobi approach”. English. In: *Ann. Inst. Fourier* 71.4 (2021), pp. 1733–1755. ISSN: 0373-0956. DOI: 10.5802/aif.3433.
- [12] Brian Charlesworth. “Effective population size and patterns of molecular evolution and variation”. In: *Nature Reviews Genetics* 10.3 (2009), pp. 195–205.
- [13] A. Cortines and B. Mallein. “A N -branching random walk with random selection”. English. In: *ALEA, Lat. Am. J. Probab. Math. Stat.* 14.1 (2017), pp. 117–137. ISSN: 1980-0436. URL: alea.impa.br/articles/v14/14-07.pdf.
- [14] Aser Cortines and B. Mallein. “The genealogy of an exactly solvable Ornstein-Uhlenbeck type branching process with selection”. English. In: *Electron. Commun. Probab.* 23 (2018). Id/No 98, p. 13. ISSN: 1083-589X. DOI: 10.1214/18-ECP197.
- [15] Jón Danielsson. “The emperor has no clothes: Limits to risk modelling”. In: *Journal of Banking & Finance* 26.7 (2002), pp. 1273–1296.
- [16] R. Durrett. *Probability models for DNA sequence evolution*. Vol. 2. Springer, 2008.
- [17] F. Duveau et al. “Fitness effects of altering gene expression noise in *Saccharomyces cerevisiae*”. In: *Elife* 7 (2018), e37272.
- [18] N. Eling, M. D Morgan, and J. C. Marionni. “Challenges in measuring and understanding biological noise”. In: *Nature Reviews Genetics* 20.9 (2019), pp. 536–548.
- [19] D. S. Falconer. *Introduction to quantitative genetics*. Pearson Education India, 1996.

- [20] R. A Fisher. “XXI.—On the dominance ratio”. In: *Proceedings of the royal society of Edinburgh* 42 (1923), pp. 321–341.
- [21] R. A. Fisher. *The genetical theory of natural selection: a complete variorum edition*. Oxford University Press, 1923.
- [22] F. Foutel-Rodier, E. Schertzer, and J. Tourniaire. “Convergence of spatial branching processes to α -stable CSBPs: Genealogy of semi-pushed fronts”. In: *arXiv preprint arXiv:2402.05096* (2024).
- [23] S. Gavrilets and A. Hastings. “A quantitative-genetic model for selection on developmental noise”. In: *Evolution* 48.5 (1994), pp. 1478–1486.
- [24] C. A. E. Goodhart. “Problems of Monetary Management: The UK Experience”. In: *Monetary Theory and Practice*. Macmillan Education UK, 1984, pp. 91–121. ISBN: 9781349172955. DOI: 10.1007/978-1-349-17295-5_4. URL: http://dx.doi.org/10.1007/978-1-349-17295-5_4.
- [25] J. B. S. Haldane. “A mathematical theory of natural and artificial selection, part V: selection and mutation”. In: *Mathematical Proceedings of the Cambridge Philosophical Society*. Vol. 23. 7. Cambridge University Press. 1927, pp. 838–844.
- [26] J. B. S. Haldane and S. D. Jayakar. “Polymorphism due to selection of varying direction”. In: *Journal of Genetics* 58 (1963), pp. 237–242.
- [27] Oskar Hallatschek. “The noisy edge of traveling waves”. In: *Proceedings of the National Academy of Sciences* 108.5 (2011), pp. 1783–1787.
- [28] C. A. Hennessy and C. A. E. Goodhart. “Goodhart’s Law and Machine Learning: a Structural Perspective”. In: *International Economic Review* 64.3 (Apr. 2023), pp. 1075–1086. ISSN: 1468-2354. DOI: 10.1111/iere.12633. URL: <http://dx.doi.org/10.1111/iere.12633>.
- [29] W. G. Hill and H. A. Mulder. “Genetic analysis of environmental variation”. In: *Genetics research* 92.5-6 (2010), pp. 381–395.
- [30] S. K. Hortsch and A. Kremling. “Characterization of noise in multistable genetic circuits reveals ways to modulate heterogeneity”. In: *PloS one* 13.3 (2018), e0194779.
- [31] Y. Ito et al. “How selection affects phenotypic fluctuation”. In: *Molecular Systems Biology* 5.1 (2009), p. 264.
- [32] J. Karwowski et al. *Goodhart’s Law in Reinforcement Learning*. 2023. arXiv: 2310.09144 [cs.LG]. URL: <https://arxiv.org/abs/2310.09144>.
- [33] L. Keren et al. “Massively parallel interrogation of the effects of gene expression levels on fitness”. In: *Cell* 166.5 (2016), pp. 1282–1294.
- [34] H. Kesten. “Branching Brownian motion with absorption”. English. In: *Stochastic Processes Appl.* 7 (1978), pp. 9–47. ISSN: 0304-4149. DOI: 10.1016/0304-4149(78)90035-2.
- [35] V. Koltun and D. Hafner. “The h-index is no longer an effective correlate of scientific reputation”. In: *PLoS One* 16.6 (2021). DOI: 10.1371/journal.pone.0253397.
- [36] R. Lande. “Quantitative genetic analysis of multivariate evolution, applied to brain: body size allometry”. In: *Evolution* (1979), pp. 402–416.
- [37] R. C. Lewontin. “The units of selection”. In: *Annual review of ecology and systematics* 1.1 (1970), pp. 1–18.
- [38] B. Mallein. “ N -branching random walk with α -stable spine”. English. In: *Theory Probab. Appl.* 62.2 (2018), pp. 295–318. ISSN: 0040-585X. DOI: 10.1137/S0040585X97T988611.
- [39] Alexander Pan, Kush Bhatia, and Jacob Steinhardt. “The Effects of Reward Misspecification: Mapping and Mitigating Misaligned Models”. In: *International Conference on Learning Representations*. 2022. URL: <https://openreview.net/forum?id=JYtwGwIL7ye>.
- [40] C. Pelabon et al. “Evolution of variation and variability under fluctuating, stabilizing, and disruptive selection”. In: *Evolution* 64.7 (2010), pp. 1912–1925.

- [41] J. Pitman. “Coalescents with Multiple Collisions”. In: *The Annals of Probability* 27.4 (1999), pp. 1870–1902. ISSN: 00911798. URL: <http://www.jstor.org/stable/2652847>.
- [42] Matthew I. Roberts and Jason Schweinsberg. “A Gaussian particle distribution for branching Brownian motion with an inhomogeneous branching rate”. English. In: *Electron. J. Probab.* 26 (2021). Id/No 103, p. 76. ISSN: 1083-6489. DOI: 10.1214/21-EJP673.
- [43] E. Schertzer and J. Tourniaire. “Spectral analysis and k -spine decomposition of inhomogeneous branching Brownian motions. Genealogies in fully pushed fronts”. In: *arXiv preprint arXiv:2301.01697* (2023).
- [44] E. Schertzer and A. H. Wences. “Relative vs absolute fitness in a population genetics model. how stronger selection may promote genetic diversity”. In: *arXiv preprint arXiv:2301.07762* (2023).
- [45] J. M. Smith and J. Haigh. “The hitch-hiking effect of a favourable gene”. In: *Genetics Research* 23.1 (1974), pp. 23–35.
- [46] J. Tourniaire. “A branching particle system as a model of semi pushed fronts”. In: *arXiv preprint arXiv:2111.00096* (2021).
- [47] J. Viñuelas et al. “ToW.s experimental manipulation of stochasticity in gene expression”. In: *Progress in biophysics and molecular biology* 110.1 (2012), pp. 44–53.

Supplemental Materials for: The interplay between natural selection and evolution: a fitness wave approach

Outline

We present in this Supplementary material the mathematical analysis of the model described in Section 2 of the main text. We first describe in more details in Section S.1 the properties of the sequence (g_n, p_n) of genotypic and phenotypic profiles that will be proved in this text, both regarding the traveling wave solutions of the dynamic (4.2) and the genealogical properties of the underlying model.

These results are then prove in the next three sections of the Supplementary material. We describe in Section S.2 some a priori results on the profile dynamic, including regularization properties and the preservation of the concavity. These estimates are used in Section S.3 to identify the traveling wave solutions to the dynamic, and in Section S.4 to describe the genealogical relationships of individuals in the model.

In Section S.5, we provide heuristics for the rate of convergence of the stochastic profile of the population model towards their hydrodynamic-type limits. This convergence appear to be particularly slow, however, numerical simulations show that the phase transition observed for the deterministic dynamic of fronts is also well-marked for finite size populations. Finally, Section S.6 discusses the extensions of our results to population models with sexual reproduction, highlighting the main differences between sexual and asexual models.

S.1 Main results

Let us recall that in the main article, we introduced a finite size branching-selection population model, in which individuals give birth to a large number of children, with a genotype inherited from their parent with a random increment, and a phenotype given by a random increment of their genotype. The selection procedure applies on the phenotypes. We observed that in the large population limit, the evolution of this system is well-described by a family of phenotypic and genotypic profiles p_n and g_n , corresponding respectively to the distribution of phenotype among the children of the n -1st generation and the distribution of genotype among the selected individuals that make the n th generation. We recall that the profiles (p_n, g_n) evolve according to the following deterministic recursive dynamic

$$\begin{aligned} p_n(x) &= \pi \left[1 - \gamma + \sup_{y \in \mathbb{R}} (g_{n-1}(y) - \min(1, \mu)(x - y)_+) \right] \\ s_n &= \sup \{x \in \mathbb{R} : p_n(x) \geq \gamma\} \\ g_n(x) &= \pi \left[1 - \gamma + \sup_{y \in \mathbb{R}} (g_{n-1}(y) - |x - y| - \mu(s_n - x)_+) \right], \end{aligned} \tag{S.1.1}$$

with $\pi : x \in \mathbb{R} \mapsto x \mathbb{1}_{\{x \geq 0\}} - \infty \mathbb{1}_{\{x < 0\}}$.

We discuss in the forthcoming Section S.1.1 the existence and properties of traveling wave solutions to this dynamic. We observe that the behaviour of these traveling wave sharply depend on the values of γ and μ , and exhibit a phase transition between two distinct behaviour, that are called *semi-pulled* and *fully-pulled*, corresponding to the strong, respectively weak, selection regime. Section S.1.1 then describe in more details the differences between these two regimes. Section S.1.3 then compare our results to the existing state of the art.

S.1.1 The traveling wave

We say that a function g is a *traveling wave* for the dynamic (S.1.1) with speed v if, starting from $g_0 = g$, for all $n \in \mathbb{N}$ we have

$$g_n : x \mapsto g(x - nv). \tag{S.1.2}$$

In other words, the dynamic has the effect of shifting the genotypic profile by v , without deformation. Given the definition of profiles, we refer to the *support* of the traveling wave g as $g^{-1}(\mathbb{R}_+)$, the set of points x such that $g(x) \geq 0$. That is, x is in the support of g , if there will be individuals in the neighbourhood of $x \log N$ with high probability, when N is large enough.

Our main result is stated in the theorem below, which shows existence and uniqueness of a traveling wave solution to (S.1.1). The proof of this theorem can be found at the end of Section S.3.

Theorem S.1.1. *For all $\gamma \in (0, 1)$ and $\mu \in \mathbb{R}_+ \setminus \{1\}$, we set $k = \lfloor 1/\mu \rfloor$. For the dynamic described in (S.1.1), there exists a unique up to translation, concave traveling wave g with compact support. This traveling wave has speed $v(\gamma, \mu)$ given by*

$$v(\gamma, \mu) = \begin{cases} \frac{2\gamma}{k(2-(k+1)\mu)} & \text{if } \gamma \leq \gamma_c(\mu) \\ 1 - \gamma & \text{if } \gamma > \gamma_c(\mu) \end{cases}, \quad \text{where } \gamma_c(\mu) = \frac{k}{k+1} \left(1 - \frac{\mu}{2-k\mu}\right).$$

In particular, the function $\gamma \mapsto v(\gamma, \mu)$ is increasing on the interval $(0, \gamma_c]$ and decreasing on $[\gamma_c, 1)$, whereas the function $\mu \mapsto v(\gamma, \mu)$ is increasing.

It is worth mentioning that in the above theorem, if $\mu > 1$ then $k = 0$. Therefore, $\gamma_c(\mu) = 0$ for all $\mu > 1$. This indicates that if the tail of the phenotypic contribution is light enough, then the phase transition between the weak selection and the strong selection regimes does not occur. More precisely, the population is always in the weak selection regime, and decreasing the value of γ increases the rate of adaptation of the population. This behaviour is a consequence of the fact that in this regime, the phenotypic value of an individual is very close to its genotypic value, so the phenotypic and genotypic selection procedures become essentially undistinguishable.

Remark. If $\mu = 1$, then the law of $X/(c \log N)$ conditionally on $X + Y > c \log N$ converges in distribution to a uniform random variable on $[0, 1]$, therefore the relationship between phenotype and genotype of an individual cease to be well-concentrated around a deterministic value. We do not treat this limiting case in the present paper although the formula we obtained can be prolonged by continuity at $\mu = 1$.

The proof of Theorem S.1.1 is based on the explicit construction of the traveling waves associated to the parameters (γ, μ) . The traveling wave will typically be formed as a concave, piecewise linear function whose maximum is γ . The slope near the right edge of the traveling wave is either -1 or $\mu - 1$ depending on whether $\gamma \leq \gamma_c$ or $\gamma > \gamma_c$. This slope relates to the exponential growth of the size of the population with a genotype at distance smaller than $x \log N$ from the largest genotype of a given generation, for x small enough.

As stated in the theorem, for a fixed value of μ , the speed of the traveling wave (corresponding to the rate of adaptation of the population) takes its maximum at a critical value of $\gamma = \gamma_c(\mu)$ (corresponding to an optimal choice of the selection pressure). The function $\mu \mapsto \gamma_c(\mu)$ is drawn on the left panel of Fig. 3 in the main text, together with empirical estimates of the optimal choice of γ for various finite size population models.

In particular, if $\mu > 1$, i.e. if a large increment of phenotype in an individual is primarily explained by a large increment of its genotype, the optimal selection pressure is obtained as $\gamma = 0$, i.e. a maximal selection pressure. In this situation, the optimal dynamic for the population is to select at every step a constant (independent of N) number of individuals with the largest phenotype at each generation to maximize the rate of adaptation of the population. The maximal genotype in the population will increase by $\log N$ in each generation, which is similar to the Brunet-Derrida behaviour obtained for the exponential model of branching random walk with selection [10, 38] introduced in Section S.1.3.

On the other hand, if $\mu < 1$, i.e. if individuals can have a very high phenotype without having a large genotype, there exists a non-trivial optimum for the selection pressure at $\gamma = \gamma_c$. This selection pressure gives an optimal rate of adaptation of the population, by ensuring that the selection step keeps individuals with high genotypic value and makes them create a large enough number of children so that their characteristics are transmitted to their descendants.

Convergence to the traveling wave

Theorem S.1.1 shows the existence and uniqueness of a traveling wave solution to the dynamic (S.1.1). Proving that, starting from an arbitrary genotypic profile (satisfying some conditions), the dynamic converges to the traveling wave solution is out of the scope of this paper. However, simulations in the top right panel of Fig. 2 in the main text indicate that we should indeed have convergence, and therefore a detailed analysis of the traveling waves is needed to describe the long term behaviour of the dynamical system (S.1.1).

S.1.2 Fully-pulled and semi-pulled waves

Assuming that $\mu < 1$, the properties of the traveling wave solution are quite different depending on whether $\gamma > \gamma_c$ or $\gamma \leq \gamma_c$. These differences can be explained through the genealogical relationships and selection properties appearing at the front of the population. When we refer to the front of the population, we mean the genotypes within a positive but not too large distance from the rightmost genotype (on the logarithmic scale). By the tip of the profile we understand particles located at or very near the rightmost position (on the logarithmic scale). Our terminology for the traveling waves refers to the fact that the front of the fully-pulled wave is generated by the tip (i.e. genotypes at the front have parents at the tip), and in the semi-pulled case the front is generated by parents at the front but not necessarily at the tip.

Ancestry

Our method to find the most likely location of the parent of a genotype at a given location (for example at the front) is to study A , the ancestral function of the process. Suppose that g is a traveling wave solution to (S.1.1) with speed v and with $g^{-1}(\mathbb{R}_0^+) = [L, 0]$ for some $L < 0$. We define

$$A : x \in [L, 0] \mapsto \operatorname{argmax}_{y \in \mathbb{R}} \{g(y) - |x + v - y|\},$$

where for any concave function $u : \mathbb{R} \rightarrow \mathbb{R} \cup \{-\infty\}$, $\operatorname{argmax}_{y \in \mathbb{R}} \{u(y)\}$ returns the *smallest* real number y such that $u(y) = \max_{z \in \mathbb{R}} u(z)$. Given the heuristics behind the definition of the dynamic (S.1.1), we see that $A(x)$ corresponds to the distance from the tip of the genotypic value of a typical parent of an individual at distance x from the tip. Note that $A^j(x)$ then describes the distance from the tip for a typical ancestor j generations in the past, in a population distributed according to the traveling wave.

For a better illustration of the difference between fully-pulled and semi-pulled regimes, we also introduce the function A^+ , as

$$A^+ : x \in [L, 0] \mapsto \operatorname{Argmax}_{y \in \mathbb{R}} \{g(y) - |x + v - y|\},$$

where for any concave function $u : \mathbb{R} \rightarrow \mathbb{R} \cup \{-\infty\}$, $\operatorname{Argmax}_{y \in \mathbb{R}} \{u(y)\}$ returns the *largest* real number y such that $u(y) = \max_{z \in \mathbb{R}} u(z)$. Now the theorem below says that, when $\gamma \leq \gamma_c$ (fully-pulled case), then a typical ancestor of an individual finitely many generations in the past, will be at the very tip of the population. On the other hand, if $\gamma > \gamma_c$ (semi-pulled case), a typical ancestor will be located in an interval at the front. In this case $A^j(x)$ and $(A^+)^j(x)$ will not agree as j gets large, and the length of the interval will be given by $(A^+)^j(x) - A^j(x)$ for some large $j \in \mathbb{N}$. We will prove this theorem in Section S.4.

Theorem S.1.2. *The functions $x \mapsto A(x)$ and $x \mapsto A^+(x)$ are non-decreasing. Moreover:*

- If $\gamma \leq \gamma_c$, then $A^j(x) = A^{+j}(x) = 0$ for all j large enough;
- If $\gamma > \gamma_c$, then there exists $c_1 > 0$ such that $A^j(x) = -c_1$ and $A^{+j}(x) = 0$ for all j large enough.

Remark. Let $\gamma > \gamma_c$, we write g the associated traveling wave. We observe that the parameter c_1 defined above, corresponding to the lowest fitness ancestor that can give birth to one individual at the front of the population verifies $g(c_1) < \gamma$. In other words, ancestors of the fittest individuals never come from the bulk of the process (which are the majority of individuals, whose fitness is very close to $\sup\{x \in \mathbb{R} : g(x) = \gamma\}$).

In other words, in the strong selection regime $\gamma < \gamma_c$, the whole population is generated by the tip of the process a finite number of generations backward in time with high probability. In this regime, the individuals with highest genotype at a given generation will generate the whole rest of the population within a finite number of generations. On the other hand, in the weak selection regime $\gamma > \gamma_c$, the population is generated by a group of ancestors consisting of the N^{c_1} individuals with highest genotype. Coalescences within this group of ancestor then occur on a much slower, logarithmic rate, leading to the age of the most recent common ancestor of the population to be of order $\log N$, compared to a constant in the other regime.

Selection properties

The next important property, which distinguishes the fully-pulled and semi-pulled traveling waves is the following. Let us consider the set of genotypes at the moment when reproduction has already happened, but selection has not. Then in the fully-pulled regime ($\gamma \leq \gamma_c$), the best (largest) genotypes do not survive the selection step, whereas in the semi-pulled case ($\gamma > \gamma_c$) they do.

In order to state this result precisely, we need to introduce the reproduction profile. Let g be a traveling wave solution with speed v , and assume $g^{-1}(\mathbb{R}_0^+) = [L, 0]$ for some $L < 0$. Then, since g is a traveling wave, if $g_0 = g$ then $g_1(x) = g(x - v)$, and $g_1^{-1}(\mathbb{R}_0^+) = [L + v, v]$. Now similarly to the heuristics given for the dynamics (S.1.1), we define the reproduction profile

$$r(x) := \pi \left[1 - \gamma + \sup_{y \in \mathbb{R}} (g(y) - |x - y|) \right],$$

which describes the log-density of genotypes after reproduction and before selection. The result below says that, if $\gamma < \gamma_c$, then the right edge of the support of the function r is to the right of v , which is the right edge of the support of the function g_1 . That is, the largest genotypes after reproduction (the ones to the right of v) do not survive selection. On the other hand, when $\gamma > \gamma_c$ then the functions g_1 and r agree on an interval at the front of these profiles (the best genotypes are among the selected ones). We prove this theorem at the end of Section S.3.

Theorem S.1.3. *Recall that r is the log-density profile of phenotypes of children of a population with genotypic profile g , and the genotypic profile of the surviving children is g_1 . Then:*

- *If $\gamma < \gamma_c$ then $r(x) > g_1(x)$ for all x in the support of g_1 .*
- *If $\gamma > \gamma_c$ then $r(x) = g_1(x)$ for all x close enough to v , the right edge of the support of g_1 .*

Summary

We now provide illustrations and a summary of the properties, which are stated in the theorems above, and which distinguish the fully-pulled and semi-pulled waves. In order to do so, let g be a traveling wave solution to (S.1.1) with speed v , and let $s := s_1$ be the phenotypic threshold at generation 1. Note that s is also the distance of the phenotypic threshold from the rightmost genotype in any generation, because of the stationarity of the profile. Let us first return to the bottom panels of Fig. 2 in the main text, which we describe in the context of the above described results.

Left Panel. Fully-pulled wave. The fact that the phenotypic threshold (red segment) s is to the right of the reproduction profile (orange) means, that any genotype that survives selection needs to perform a large phenotypic jump (of order $\log N$) to get to the right of s . Since the probability of such jumps is small, and the number of genotypes near the tip of the reproduction profile is not large enough, the very best genotypes do not survive selection. That is, the genotypic profile in the next generation (green) is to the left of the reproduction profile (orange). Furthermore, if we sample a genotype uniformly at random from the interval $[0, v]$ at time $n + 1$ (i.e. from the front of the green curve), then the most likely location of its parent will be at 0 (at the tip of the blue curve).

Right Panel. Semi-pulled wave. After reproduction (orange), all the extreme genotypes to the right of the phenotypic threshold s (red segment) are selected to the next generation: the orange and the green profiles coincide on the interval $[s, v]$. If we sample a genotype uniformly at random from

the interval $[0, v]$ at generation $n + 1$, then the most likely location of its parent will be on the interval $[s - v, 0]$ (the log-density of this interval is given by the first linear segment of the blue curve, which has slope 1).

In the table below, we give a summary of the main properties of the investigated traveling waves. The facts that in the fully-pulled case ($\gamma \leq \gamma_c$) we have $v \leq s$, and in the semi-pulled case ($\gamma > \gamma_c$) we have $v > s$ are stated and proved in Section S.3.

Table 1: Comparison of the phenomenological picture between the full-pulled and semi-pulled regimes.

	Fully-pulled wave	Semi-pulled wave
	$\gamma < \gamma_c, v < s$	$\gamma > \gamma_c, v > s$
Stationary profile		
Speed	increasing function of γ	decreasing function of γ
Slope of g at the front	$\mu - 1$	-1
Ancestry		
Ancestral line	located near the tip	located away from both the tip and the bulk
Number of potential parents of the tip	$N^{o(1)}$	$N^{v-s+o(1)}$
Selection		
Phenotypic threshold	To the right of the rightmost selected genotype ($s > v$).	To the left of the rightmost selected genotype ($s < v$).
Probability of selection of the largest genotype	converges to 0	converges to 1

S.1.3 Related mathematical literature

A large number of population models for natural selection have been introduced over the years. These population models usually present a *fitness*, identified as a real value, that measures the ability of an individual to survive and produce a large offspring. Among these models one can find the class of *branching-selection particle systems*. These processes are defined as Markovian particle systems, in which each individual gives birth, independently to one another, to children with a fitness obtained as a random modification of their own. An external operation is then undertaken to keep the total number of individuals at each generation of roughly the same size.

One of the first of these models to be introduced was the branching random walk with absorption. In this model, individuals reproduce creating children with fitness given by an i.i.d. copy of a point process shifted by their own. Children are then killed if their fitness falls below a given threshold. Kesten [34] showed this process to be either subcritical, critical or supercritical, i.e. the population either grows extinct exponentially fast, polynomially fast, or survives and grows exponentially fast with positive probability.

To control the size of the population more accurately, Brunet and Derrida [7] introduced the so-called *N-branching random walk*. In this model, the reproduction law is identical to the previous one, each individual reproduce independently by creating an identically distributed cloud of children around their position, but at each step only the N rightmost children are selected to reproduce in the next generation. As a result, the total size of the population remains constant. By comparison to the KPP equation with a cutoff and the study of exactly solvable models by Brunet, Derrida, Mueller and Munier [10, 9], they conjectured the so-called *Brunet-Derrida behaviour* of the N -branching random walk, i.e. that the speed v_N of adaptation of the population with N individuals converges as $N \rightarrow \infty$

to the speed of adaptation of the population without selection at the slow rate

$$v_N - v_\infty \sim \frac{-K}{(\log N)^2}, \text{ where } K \text{ is an explicit positive constant.}$$

This result was later proved by Bérard and Gouéré [1] for binary branching, then extended by Mallein [38] to general branching.

The population model we introduced is analogue to an N -branching random walk –and more specifically to the exponential exactly solvable model introduced in [9]– when $\gamma \rightarrow 0$. In this case, the population is capped to a value cN for some $c < 1/2$, and each individual creates $\lfloor 1/c \rfloor$ children independently of one another. If the selection only keeps the individuals with the largest genotypic value (i.e. in the limit $\mu \rightarrow \infty$), we recover an N -branching random walk in which the displacements are given by i.i.d. Laplace steps. The case $\mu > 1$ corresponds to a situation when individuals are not necessarily selected if they are among the N rightmost, but their probability of being selected decays exponentially fast if they are far from the maximal fitness. A solvable model in this universality class was studied by Cortines and Mallein [13], that showed no noticeable difference in the evolution of the population due to this randomization.

For $\gamma > 0$, using extreme value theory, the evolution of the population we consider becomes closer to the solvable models studied in [10, 13, 14], corresponding respectively to the cases $\mu = \infty$, $\mu > 1$ and $\mu < 1$. For $\gamma > 0$ and $\mu < 1$, Schertzer and Wences [44] studied a model close to the one we consider. In their model, reproduction happens according to a Poisson point process, and noisy selection is performed via Gibbs sampling. One of the surprising outcomes of that work is that genetic diversity (or effective population size) is non-monotonous in the strength of selection: there is a phase transition between weak and strong selection regimes, and genetic diversity increases with the strength of selection in the strong selection regime.

We prove for our model a similar behavior for the rate of adaptation of the population in Theorem S.1.1. We observe that $\gamma \mapsto v(\mu, \gamma)$ is non-monotone, as can be seen in the simulations in the left panels of Fig. 1. We see that for any given value of phenotypic variance (i.e. for any given μ), there is a critical value of γ for which the speed takes its maximum.

S.2 Some a priori properties of the deterministic dynamics

In this section, we present some properties of the dynamic of (g_n, p_n) described in (S.1.1). We first remark that this dynamic preserves concavity, and that $\sup g_n = \gamma$ for any $n \geq 1$. We then use this latter observation to give an alternative description of the dynamic of the genotypic profile, defining s_n as the unique real number such that $\sup g_n = \gamma$.

We begin with the following straightforward observation.

Lemma S.2.1. *Let f, g be two concave functions $\mathbb{R} \rightarrow \mathbb{R} \cup \{-\infty\}$. The function*

$$x \mapsto \sup_{z \in \mathbb{R}} f(z) + g(x - z)$$

is concave.

This result can be viewed as a property of a tropicalized version of the convolution. Similarly to the fact that log-concavity is preserved by the convolution operation, concavity is preserved by the tropicalized convolution operation.

Proof. Let $t \in (0, 1)$. Using the concavity of f and g , for $x, x' \in \mathbb{R}$ we have

$$\begin{aligned} \sup_{z \in \mathbb{R}} f(z) + g(tx + (1-t)x' - z) &= \sup_{(z, z') \in \mathbb{R}^2} f(tz + (1-t)z') + g(t(x - z) + (1-t)(x' - z')) \\ &\leq t \sup_{z \in \mathbb{R}} f(z) + g(x - z) + (1-t) \sup_{z' \in \mathbb{R}} f(z') + g(x' - z'), \end{aligned}$$

which shows the result. □

By Lemma S.2.1, the concavity of g_n is preserved by the dynamic.

Proposition S.2.2. *Let g_0 be a concave function, and (g_n, p_n) defined recursively by (S.1.1) for all $n \geq 1$. For all $n \geq 1$, p_n and g_n are concave.*

Remark. This result justifies the choice of only considering concave traveling waves. If the population starts from a log-concave initial distribution of genotypes, then the distribution of genotypes remains log-concave at all steps.

Proof. We first show that g_n and p_n are concave for any $n \geq 1$. Assuming that g_{n-1} is concave, then by Lemma S.2.1, the function

$$\bar{p}_n : x \mapsto 1 - \gamma + \sup_{y \in \mathbb{R}} g_{n-1}(y) - \min(1, \mu)|x - y|$$

is concave, using the concavity of $z \mapsto -\min(1, \mu)|z|$. Then, using that π is concave and increasing, we conclude that $p_n = \pi \circ \bar{p}_n$ is concave. Similarly,

$$\bar{g}_n : x \mapsto 1 - \gamma + \sup_{y \in \mathbb{R}} g_{n-1}(y) - |x - y| - \mu(s_n - x)_+,$$

is concave, using Lemma S.2.1 again and the fact that $x \mapsto -\mu(s_n - x)_+$ is concave. As a result, $g_n = \pi \circ \bar{g}_n$ is concave. \square

For any $g : \mathbb{R} \rightarrow \mathbb{R} \cup \{-\infty\}$ and $\xi \in \mathbb{R}$, we define the functional

$$\Phi_\xi[g] : x \mapsto 1 - \gamma + \sup_{y \in \mathbb{R}} g(y) - |x - y| - \mu(\xi - x)_+. \quad (\text{S.2.1})$$

We remark that for all $n \in \mathbb{N}$, we have $\pi \circ \Phi_{s_n}[g_{n-1}] = g_n$. Therefore, defining the value of s_n from g_{n-1} would allow us to rewrite the dynamic (S.1.1) without reference to the phenotypic profile. This is the objective of the following lemma.

Lemma S.2.3. *Let g be a function $\mathbb{R} \rightarrow \mathbb{R} \cup \{-\infty\}$. The function*

$$F : \xi \mapsto \sup_{x \in \mathbb{R}} \Phi_\xi[g](x)$$

is non-increasing.

Proof. By immediate computations, we have

$$\sup_{x \in \mathbb{R}} -|x - y| - \mu(\xi - x)_+ = \begin{cases} -\mu(\xi - y)_+ & \text{if } \mu < 1 \\ -(\xi - y)_+ & \text{if } \mu > 1. \end{cases}$$

Therefore, for $\xi \in \mathbb{R}$, we have

$$F(\xi) = 1 - \gamma + \sup_{(x,y) \in \mathbb{R}^2} g(y) - |x - y| - \mu(\xi - x)_+ = 1 - \gamma + \sup_{y \in \mathbb{R}} g(y) - \min(\mu, 1)(\xi - y)_+.$$

Using that $\xi \mapsto -\min(\mu, 1)(\xi - y)_+$ is non-increasing for all $y \in \mathbb{R}$, we conclude that F is non-increasing as well. \square

We are now able to state the alternative construction of the deterministic dynamic of the genotypic profile.

Proposition S.2.4. *Let $g_0 : \mathbb{R} \rightarrow \mathbb{R} \cup \{-\infty\}$ be such that $\sup g_0 = \gamma$. Let (s_n) and (g_n) be the quantities defined recursively in (S.1.1). For all $n \geq 1$, we have*

$$\begin{aligned} s_n &= \sup\{\xi \in \mathbb{R} : \sup_{x \in \mathbb{R}} \Phi_\xi[g_{n-1}](x) \geq \gamma\}, \\ g_n &= \pi \circ \Phi_{s_n}(g_{n-1}). \end{aligned} \quad (\text{S.2.2})$$

Proof. We remark from the proof of Lemma S.2.3 that for any $n \geq 0$, we have

$$\sup_{x \in \mathbb{R}} \Phi_\xi[g](x) = p_{n+1}(\xi),$$

therefore we have $s_{n+1} = \sup\{\xi \in \mathbb{R} : \sup_{x \in \mathbb{R}} \Phi_\xi[g_n](x) \geq \gamma\}$ by (S.1.1). The formula for g_{n+1} follows immediately by (S.1.1), and we complete the proof. \square

We complete this section by remarking that for all $n \geq 1$, the slope of g_n is bounded by -1 on $\{x \in \mathbb{R} : g_n(x) \geq 0\}$. More precisely, we prove the following result.

Lemma S.2.5. *Let $g : \mathbb{R} \rightarrow \mathbb{R} \cup \{-\infty\}$ and $\xi \in \mathbb{R}$. Then the function $x \mapsto \Phi_\xi[g](x) + x$ is non-decreasing.*

Proof. For all $x \in \mathbb{R}$, we have

$$\begin{aligned} \Phi_\xi[g](x) + x &= 1 - \gamma + \sup_{y \in \mathbb{R}} (g(y) - |y - x| + x) - \mu(\xi - x)_+ \\ &= 1 - \gamma + \sup_{y \in \mathbb{R}} (g(y) + y - 2(y - x)_+) - \mu(\xi - x)_+. \end{aligned}$$

As $x \mapsto -\mu(\xi - x)_+ - 2(y - x)_+$ is non-decreasing for all $y \in \mathbb{R}$, we conclude that $x \mapsto \Phi_\xi[g] + x$ is also non-decreasing. \square

S.3 Traveling wave genotypic profiles

The main objective of the present section is to describe the concave traveling waves with compact support for the profile of our population. As we will see, these traveling waves are constructed as piecewise linear functions. Observing that there is a one-to-one map between (v, s) and (γ, μ) will then allow us to complete the proof of Theorem S.1.1.

In all the rest of this section, g will denote a concave traveling wave with speed v . Without loss of generality, up to translation of g we can assume that

$$\sup\{x \in \mathbb{R} : g(x) > 0\} = 0. \quad (\text{S.3.1})$$

We denote by L the left edge of the profile,

$$L := \inf\{x \in \mathbb{R} : g(x) > 0\}, \quad (\text{S.3.2})$$

so that the support of g is $[L, 0]$, and (by concavity) we have $g(x) = -\infty$ if $x \notin [L, 0]$. In particular, we refer to $|L|$ as the width of g .

Recalling the definition of the functional Φ from (S.2.1), we also define

$$s := \sup\{\xi \in \mathbb{R} : \sup_{x \in \mathbb{R}} \Phi_\xi[g](x) \geq \gamma\}, \quad (\text{S.3.3})$$

which plays the role of the phenotypic threshold in a population starting with a genotypic profile g . In particular, g being a traveling wave, we have

$$\forall x \in \mathbb{R}, \quad g(x) = \pi(\Phi_s[g](x + v)).$$

Observe that $x \mapsto \Phi_s[g](x + v)$ is a concave function $\mathbb{R} \rightarrow \mathbb{R}$ by Lemma S.2.1. It is in particular continuous, therefore $g(0) = g(L) = 0$, using that π is upper semi-continuous. Therefore, the above equation can be rewritten as

$$\forall x \in [L, 0], \quad g(x) = \Phi_s[g](x + v). \quad (\text{S.3.4})$$

Now we state the main result of this section, which is a more precise version of Theorem S.1.1. We describe the fully-pulled ($\gamma \leq \gamma_c$) and semi-pulled ($\gamma > \gamma_c$) traveling wave solutions to (S.1.1) as piecewise linear functions.

Theorem S.3.1. *Let $\gamma \in (0, 1)$ and $\mu \in \mathbb{R}_+ \setminus \{1\}$, we set $k := \lfloor 1/\mu \rfloor$ and $K := \lfloor 2/\mu \rfloor$. Then there exists a unique up to translation, concave, compactly supported traveling wave g to the dynamic (S.1.1). Writing $[L, 0]$ for the support of g , the function is differentiable everywhere on $[L, 0]$ except for a finite number of points, and we have*

$$g : x \in \mathbb{R} \mapsto \pi \left(\int_x^0 g'(y) dy \right). \quad (\text{S.3.5})$$

Moreover, we can identify g' on the interval $[L, 0]$ as follows. Let $v := v(\gamma, \mu)$ and s as defined in (S.3.3).

- If $\gamma < \gamma_c$, then for all $x \in [L, 0]$ we have

$$g'(x) = (j\mu - 1), \quad \text{if } -jv < x < -(j-1)v \text{ for some } j \geq 1, \quad (\text{S.3.6})$$

where

$$v = \frac{2\gamma}{k(2 - (k+1)\mu)} \leq s.$$

- If $\gamma > \gamma_c$, then for all $x \in [L, 0]$, we have

$$g'(x) = \begin{cases} -1, & \text{if } x > s - v \\ (j\mu - 1), & \text{if } s - (j+1)v < x < s - jv \text{ for some } 1 \leq j \leq K+1 \\ 1 + \mu, & \text{if } x < s - (K+2)v, \end{cases} \quad (\text{S.3.7})$$

where

$$v = 1 - \gamma \quad \text{and} \quad v - s = 1 - (1 - \gamma) \left(k \left(1 - \frac{k+1}{2} \mu \right) + 1 \right) =: \chi(\mu, \gamma) > 0. \quad (\text{S.3.8})$$

In particular, $\gamma \mapsto v(\mu, \gamma)$ changes monotonicity at $\gamma_c(\mu)$ and is maximized at that point.

We first collect specific properties of the traveling wave g , which will be used in the proof of Theorem S.3.1. We will write

$$m = \operatorname{argmax}(g) \in (L, 0)$$

for the leftmost point at which g attains its maximum. By Lemma S.2.3 and (S.1.2), we remark that $g(m) = \sup g = \gamma$, so m corresponds to the genotypic value shared by the largest portion of the population. Moreover, by concavity of g , we conclude that g is increasing on $(-\infty, m]$ and non-decreasing on $[m, \infty)$.

The following notation will also be useful. If there exists $x \in (L, 0)$ such that $g'(x) > 1$, then let d denote the unique negative real number such that $g' > 1$ on the interval (L, d) and $g' \leq 1$ on (d, ∞) . Furthermore, if $g' \leq 1$ on the interval $(L, 0)$, then we define $d := L$. Now $d < 0$ is well-defined because of the concavity of g .

Lemma S.3.2. *The function $y \mapsto g(y) + y$ is non-decreasing on the interval $(-\infty, 0]$, and the function $y \mapsto g(y) - y$ is non-increasing on the interval $[d, \infty)$ and increasing on $[L, d]$.*

Proof. As $g(x) = \pi \circ \Phi_s[g](x + v)$, the fact that $y \mapsto g(y) + y$ is non-decreasing on $(-\infty, 0]$ follows from Lemma S.2.5 and our convention that g is non-negative on $[L, 0]$ only. The second part follows from the definition of d . \square

Using the definition of Φ_s immediately implies the following corollary.

Corollary S.3.3. *For all $x \geq L$, we have*

$$\Phi_s[g](x) = \begin{cases} 1 - \gamma - x - \mu(s - x)_+ & \text{if } x > 0 \\ 1 - \gamma + g(x) - \mu(s - x)_+ & \text{if } d \leq x \leq 0 \\ 1 - \gamma + g(d) - (d - x) - \mu(s - x)_+ & \text{if } x < d \end{cases} \quad (\text{S.3.9})$$

Proof. We recall that

$$\Phi_s[g](x) = 1 - \gamma - \mu(s - x)_+ + \sup_{y \in \mathbb{R}} g(y) - |x - y|.$$

Let $x \geq d$. By Lemma S.3.2, and since $g \equiv -\infty$ on $\mathbb{R} \setminus [L, 0]$, we have that the function $y \mapsto g(y) - (x - y)$ is non-decreasing on the interval $(-\infty, x \wedge 0)$, and $y \mapsto g(y) + (x - y)$ is non-increasing on (x, ∞) . We conclude that

$$\sup_{y \in \mathbb{R}} g(y) - |x - y| = \begin{cases} g(0) - |x| & \text{if } x > 0 \\ g(x) & \text{if } x \leq 0, \end{cases}$$

which completes the proof for $x \geq d$.

Now let $L \leq x < d$. Using Lemma S.3.2 again, we see that the functions $y \mapsto g(y) - (x - y)$ and $y \mapsto g(y) + (x - y)$ are non-decreasing on the intervals $(-\infty, x]$ and (x, d) respectively; and we also have that the function $y \mapsto g(y) + (x - y)$ is non-increasing on the interval $[d, \infty)$. Therefore, we obtain

$$\sup_{y \in \mathbb{R}} g(y) - |x - y| = g(d) - (d - x),$$

and the result follows. \square

Observe that from (S.3.4), we have

$$g(x - v) = \pi \circ \Phi_s[g](x)$$

for all $x \in \mathbb{R}$. In particular, as the right edge of the support of g is 0, we conclude that

$$v = \sup\{x \in \mathbb{R} : \Phi_s[g](x) \geq 0\}.$$

We finish by showing that there is no concave compactly supported stationary wave, i.e. all traveling waves have positive speed. In view of the previous corollary, we obtain a noteworthy relationship between v and s .

Lemma S.3.4. *We have $v > 0$, moreover*

$$v = \begin{cases} \frac{1-\gamma-\mu s}{1-\mu} & \text{if } v \leq s \\ 1 - \gamma & \text{if } v > s. \end{cases}$$

Proof. We write

$$p(x) = 1 - \gamma + \sup_{y \in \mathbb{R}} g(y) - \min(\mu, 1)(x - y)_+$$

for the phenotypic profile of a population starting with a genotypic profile g . From (S.1.1), we recall that $p(s) = \gamma$. Recall also the definition of the functional Φ_s from (S.2.1).

We first assume that $\mu > 1$ and $s \geq 0$. Then, by the definitions of the functions p and $\Phi_s[g]$, and since the support of g is the interval $[L, 0]$, we have $\Phi_s[g](s) = p(s) = \gamma \geq 0$. Thus, (4.4) implies that $g(s - v) = \gamma$. Using that $g(x) > 0$ if and only if $x \in (L, 0)$, we conclude that $0 < s < v$.

Next, assume that $\mu > 1$ and $s < 0$. In this case, for all $x \in (0, |s|)$, we have

$$\Phi_s[g](x) = 1 - \gamma + \sup_{y \in \mathbb{R}} g(y) - |x - y| \geq 1 - \gamma - x.$$

Therefore $\Phi_s[g](x) > 0$ for $x > 0$ small enough, in particular v is positive.

We now assume that $\mu < 1$, and first show that in this case, we have $s < \frac{1-\gamma}{\mu}$. Indeed, if this is not the case then $s \geq \frac{1-\gamma}{\mu} > 0$, and we have

$$\gamma = p_1(s) = 1 - \gamma + \sup_{y \in \mathbb{R}} g(y) - \mu(s - y)_+ \leq 1 - \gamma - \mu s + \sup_{y \leq 0} g(y) + \mu y < \sup_{y \leq 0} g(y),$$

which leads to a contradiction as $\sup_{y \leq 0} g(y) = \gamma$. However, since $s < \frac{1-\gamma}{\mu}$, then by (S.3.9), we have

$$\Phi_s[g](0) = 1 - \gamma - \mu(s)_+ > 0,$$

therefore $\Phi_s[g](x) > 0$ for x small enough, proving again that $v > 0$.

Now, as $v > 0$, it is defined as the unique positive root of the equation $\Phi_s[g](x) = 0$. By (S.3.9), this equation can be rewritten

$$1 - \gamma - v - \mu(s - v)_+ = 0.$$

Therefore, if $v > s$, we have $v = 1 - \gamma$, while if $v < s$ then $v = \frac{1 - \gamma - \mu s}{1 - \mu}$, completing the proof. \square

In the rest of the section, we identify the function g in terms of v and s . More precisely, we first assume that $v \leq s$, which we call the *fully-pulled regime*, and we identify the function g in this case, as well as the associated parameters μ and γ in terms of (v, s) . We then work under the assumption that $v > s$, that we refer to as the *semi-pulled regime*. We identify once again g, γ and μ in terms of v and s . Showing that the correspondence between (v, s) and (γ, μ) is bijective, this is enough to prove Theorem S.3.1.

Proposition S.3.5 (Characterization of fully-pulled traveling waves). *Let g be a traveling wave with speed v . Suppose that $v \leq s$. Then g is given by (S.3.5) and (S.3.6); and we have*

$$\mu < 1, \quad v = \frac{2\gamma}{k(2 - (k+1)\mu)} \quad \text{and} \quad s = \frac{1 - \gamma - (1 - \mu)v}{\mu},$$

where $k = \lfloor 1/\mu \rfloor$.

Proof. The proof mainly relies on successively describing the values of g on each interval $[-v, 0]$, $[-2v, -v]$, ..., using (S.3.9). First observe that, since $v \leq s$, for all $x \in [0, v]$ we have

$$g(x - v) = \Phi_s[g](x) = 1 - \gamma - x - \mu(s - x) = 1 - \gamma - \mu s - (1 - \mu)x.$$

In particular, g is linear on $[-v, 0]$ with slope $-(1 - \mu)$ (recall that by hypothesis, $g(0) = 0$). Recalling the notation d from Lemma S.3.2, this also shows that $d \leq -v$.

We now assume that g is affine on the interval $[-jv, -(j-1)v]$ with slope $-(1 - j\mu)$ for some $j \geq 1$ with $-jv \geq d$. We use again (S.3.9) with $x \in [-jv, -(j-1)v]$ to obtain

$$g(x - v) = \pi \circ \Phi_s[g](x) = \pi(1 - \gamma + g(x) - \mu(s - x)) = \pi(1 - \gamma - \mu s + g(x) + \mu x).$$

In other words, g is affine on $[-(j+1)v, -jv] \cap [L, 0]$ with slope $-(1 - (j+1)\mu)$. Using finite induction, and the fact that g is continuous on $[0, L]$, we conclude that g is given by (S.3.5) and (S.3.6) on $[L \vee (d - v), 0]$. Recall the notation $K = \lfloor 2/\mu \rfloor$. Then the inductive argument and the fact that $-(1 - K\mu) \leq 1$ also show that $d \leq L \vee -Kv$.

Furthermore, it can also be checked that the piecewise linear function, which takes 0 at 0 and has slopes $-(1 - j\mu)$ on the intervals $[-jv, -(j-1)v]$, is positive at $-(K-1)v$ and non-positive at $-Kv$. Together with the fact that $d \leq L \vee -Kv$, this shows that $d = L$ and that g is given by (S.3.5) and (S.3.6) on the interval $[L, 0]$.

We recall from Corollary S.3.3 that, since $v \leq s$, we have

$$v = \frac{1 - \gamma - \mu s}{1 - \mu}, \tag{S.3.10}$$

furnishing a first equation between the parameters (v, s) and (μ, γ) . To find the other one, we recall that $\sup_{y \in \mathbb{R}} g(y) = g(m) = \gamma$, which, given the formulas (S.3.5) and (S.3.6), provides a second relationship between the parameters.

More precisely, let us recall that $k = \lfloor 1/\mu \rfloor$, thus

$$k\mu \leq 1 \leq (k+1)\mu.$$

As a result, the slope of g on $[-kv, -(k-1)v]$ is $-(1 - k\mu) < 0$, while the slope of g on $[-(k+1)v, -kv]$ is $-(1 - (k+1)\mu) \geq 0$. Since g is concave, we conclude that $m = \operatorname{argmax}(g) = -kv$, and that $g(-kv) = \gamma$.

In particular, this condition implies that $k > 0$, because otherwise we would have $\gamma = g(0) = 0$. Hence, we conclude $\mu < 1$. Simple computation from (S.3.5) and (S.3.6) then yields

$$\gamma = g(-kv) = \sum_{j=1}^k v(1 - j\mu) = v \left(k - \frac{k(k+1)}{2} \mu \right),$$

therefore we obtain the second relationship

$$\gamma = \frac{kv}{2}(2 - (k+1)\mu). \quad (\text{S.3.11})$$

From (S.3.10) and (S.3.11), we deduce the conditions

$$\begin{cases} v = \frac{2\gamma}{k(2-(k+1)\mu)} \\ s = \frac{1-\gamma-(1-\mu)v}{\mu}, \end{cases} \quad (\text{S.3.12})$$

completing the proof. \square

We now turn to the study of the traveling waves associated to the semi-pushed regime.

Proposition S.3.6 (Characterization of the semi-pushed traveling waves). *Let g be a traveling wave with speed v . Suppose that $v > s$. Then, g is given by (S.3.5) and (S.3.7), and we have*

$$v = 1 - \gamma \quad \text{and} \quad s = \frac{(k+1)(1-\gamma)}{2}(2 - k\mu) - \gamma.$$

Proof. We use once again (S.3.9), first to give the value of g on the interval $[s-v, 0]$, then on each interval $[s-(j+1)v, s-jv]$ by recursion. As a first step, we show that

$$g(x) = -x \quad \text{for all } x \in [s-v, 0]. \quad (\text{S.3.13})$$

Using (S.3.9), we observe that for $x \in [s_+, v]$, we have

$$g(x-v) = \Phi_s[g](x) = 1 - \gamma - x.$$

Thus, as $v = 1 - \gamma$ by Lemma S.3.4, we have $g(x) = -x$ for all $x \in [s_+ - v, 0]$. Therefore, if $s \geq 0$, then the proof of (S.3.13) is now complete.

If $s < 0$, we prove recursively that for all $i \geq 1$ and $x \in [s_+ - iv, s_+ - (i-1)v] \cap [s-v, 0]$, we have $g(x) = -x$. This result being proved for $i = 1$, we assume it to hold for some $i \geq 1$. Then by (S.3.9), for all $x \in [s_+ - iv, s_+ - (i-1)v]$, if $x > s-v$, we have

$$g(x) = \Phi_s[g](x+v) = 1 - \gamma + g(x+v) = 1 - \gamma - (x+v) = -x,$$

proving (S.3.13) by induction. The argument also shows that $d \leq s-v$ (recall the notation d from Lemma S.3.2).

We now turn to the description of the profile of g on the interval $[s-2v, s-v]$. For all $x \in [s-v, s]$, we have

$$\begin{aligned} g(x-v) &= \Phi_s[g](x) = \begin{cases} 1 - \gamma + g(x) - \mu(s-x)_+ & \text{if } x \leq 0 \\ 1 - \gamma - x - \mu(s-x)_+ & \text{if } x > 0 \end{cases} \\ &= 1 - \gamma - x - \mu(s-x), \end{aligned}$$

showing that g has slope $-(1-\mu)$ on $[s-2v, s-v]$.

Using (S.3.9) and the same method as in the proof of Proposition S.3.5, we can again prove by induction that g has slope $-(1-j\mu)$ on $[s-(j+1)v, s-jv] \cap [L, 0]$, for all $j \leq K+1$ with $K = \lfloor 2/\mu \rfloor$. If $L < s - (K+2)v$, then we have $d = s - (K+1)v$, and by the third line of (S.3.9), the slope of g will be $1 + \mu$ on the interval $[L, s - (K+2)v]$. We therefore conclude that the traveling wave g is given by (S.3.5) and (S.3.7).

Finally, we determine the relationship between (v, s) and (μ, γ) . From (S.3.5) and (S.3.7) we see that the slope of g changes sign at $s - (k + 1)v$, and so we have $m = \operatorname{argmax}(g) = s - (k + 1)v$ and

$$\gamma = \sup g = g(s - (k + 1)v).$$

Hence, a simple computation leads to

$$\gamma = v - s + \sum_{j=1}^k v(1 - j\mu) = \frac{(k + 1)v}{2}(2 - k\mu) - s. \quad (\text{S.3.14})$$

This last equality, together with $v = 1 - \gamma$ allows us to write

$$s = \frac{(k + 1)(1 - \gamma)}{2}(2 - k\mu) - \gamma,$$

completing the proof. \square

We now have all the preliminary results needed to prove Theorem S.3.1.

Proof of Theorem S.3.1. Let $\gamma \in (0, 1)$ and $\mu > 0$. We set

$$v_f = \frac{2\gamma}{k(2 - (k + 1)\mu)} \quad \text{and} \quad v_s = 1 - \gamma,$$

as well as

$$s_f = \frac{1 - \gamma - (1 - \mu)v_f}{\mu} \quad \text{and} \quad s_s = \frac{(k + 1)(1 - \gamma)}{2}(2 - k\mu) - \gamma,$$

which are respectively the speed and phenotypic threshold of traveling waves in the fully- and semi-pulled regimes. We observe that

$$\begin{aligned} v_f \leq s_f &\iff \mu v_f \leq 1 - \gamma - (1 - \mu)v_f \iff v_f \leq 1 - \gamma \\ &\iff \frac{2\gamma}{k(2 - (k + 1)\mu)} \leq 1 - \gamma \iff \gamma \left(\frac{2}{k(2 - (k + 1)\mu)} + 1 \right) \leq 1 \\ &\iff \frac{\gamma}{\gamma_c(\mu)} \leq 1, \end{aligned}$$

and we note that these inequalities hold only if $\mu < 1$, in which case $\gamma_c(\mu) > 0$. Similarly, we have

$$\begin{aligned} v_s > s_s &\iff 1 - \gamma > \frac{(k + 1)(1 - \gamma)}{2}(2 - k\mu) - \gamma \iff \gamma(k + 1)(2 - k\mu) > (k + 1)(2 - k\mu) - 2 \\ &\iff \gamma > \frac{(k + 1)(2 - k\mu) - 2}{(k + 1)(2 - k\mu)} = \frac{k(2 - k\mu) - k\mu}{(k + 1)(2 - k\mu)} = \gamma_c(\mu). \end{aligned}$$

Moreover these inequalities hold for any $\mu \neq 1$.

If $\gamma \leq \gamma_c(\mu)$ then we have $\mu < 1$ by Proposition S.3.5, and so we also have $v_f \leq s_f$. Therefore, the traveling wave g described in Proposition S.3.5 is a solution to (S.1.2) with speed $v = v_f$. On the other hand, $\gamma \leq \gamma_c(\mu)$ also implies $v_s \leq s_s$; therefore there is no solution of the form described by Proposition S.3.6. We conclude that if $\gamma \leq \gamma_c(\mu)$ then the function given by (S.3.5) and (S.3.6) is the unique traveling wave solution to the dynamic (S.1.1) with $v = v_f \leq s$.

Similarly, if $\gamma > \gamma_c(\mu)$, we have $v_s > s_s$, thus the traveling wave g described in Proposition S.3.6 is a solution to (S.1.2) with speed $v = v_s$. Furthermore, if $\gamma > \gamma_c$ and $\mu < 1$, then $v_f > s_f$, and when $\mu > 1$, then we must have $v > s$ by Proposition S.3.5. Thus, Proposition S.3.5 does not provide any solution in this case. We conclude that, if $\gamma > \gamma_c(\mu)$, then the unique traveling wave solution to (S.1.2) is given by (S.3.5) and (S.3.7) with speed $v = v_s > s$. \square

Proof of Theorem S.1.1. This result is an immediate consequence of the more precise Theorem S.3.1. \square

Proof of Theorem S.1.3. Recall that

$$r : x \in \mathbb{R} \mapsto \pi \left[1 - \gamma + \sup_{y \in \mathbb{R}} (g(y) - |x - y|) \right]$$

denotes the reproduction profile when we start from the genotypic profile g . For any $g : \mathbb{R} \rightarrow \mathbb{R} \cup \{-\infty\}$, let us define the functional Ψ by

$$\Psi[g] : x \mapsto 1 - \gamma + \sup_{y \in \mathbb{R}} (g(y) - |x - y|),$$

so that $r(x) = \pi(\Psi[g](x))$. Now notice that

$$\Psi[g](x) = \Phi_s[g](x) + \mu(s - x)_+ \tag{S.3.15}$$

for all $x \in \mathbb{R}$, and since the function $\Phi_s[g]$ is continuous, so is $\Psi[g]$.

If $\gamma < \gamma_c$, then we have $v < s$ by Theorem S.3.1. Thus, since $\Phi_s[g](v) = 0$, (S.3.15) implies $\Psi[g](v) > 0$. Then since $\Psi[g]$ is continuous, there exists $x \in (v, s)$ such that $\Psi[g](x) > 0$ and therefore $r(x) > 0$, which concludes the first part of the theorem.

If $\gamma > \gamma_c$, then $v > s$ by Theorem S.3.1. Therefore, using (S.3.15) and the fact that $\Phi_s[g](x) \geq 0$ for all $x \in [s, v]$, we obtain

$$0 \leq g_1(x) = \Phi_s[g](x) = \Psi[g](x) = r(x),$$

for all $x \in [s, v]$, which finishes the proof. \square

S.4 Ancestral structure of the model

We now turn to the study of the ancestral structure of the population, leading to a proof of Theorem S.1.2. The main question of the section is the following: If we sample k individuals at a given time horizon, what can be inferred about the genealogical tree formed by tracing the k ancestral lineages of those individuals? As we will see, our hydrodynamic limit already offers insights into the behavior of a single ancestral lineage ($k = 1$), which will be discussed in Section S.4.1.

For multiple lineages ($k > 1$), the coalescence times are primarily influenced by the stochastic fluctuations in the system. To gain further insight, we examine an alternative individual-based model with noisy selection. Although the specifics of this model differ, this model is fully integrable and shares certain universal properties with our original selection model as the population size approaches infinity. This comparative approach will allow us to derive the ansatz for the effective population size N_e introduced in Section 4.2, and will be the focus of Section S.4.2.

S.4.1 Parental lineage

Let g be a traveling wave of speed v , and recall that the ancestral map describes the most likely location (relative to the rightmost genotype) of the parent of a uniformly chosen genotype around location x (in the log scale) 1 generation in the past:

$$A(x) := \operatorname{argmax}_{y \in \mathbb{R}} \{g(y) - |x + v - y|\},$$

where $\operatorname{argmax}_{y \in \mathbb{R}} \{g(y) - |x + v - y|\}$ is defined as the smallest y at which the maximum is attained, and

$$A^+(x) := \operatorname{Argmax}_{y \in \mathbb{R}} \{g(y) - |x + v - y|\}$$

is the largest y at which the maximum is attained. As the main step towards the proof of Theorem S.1.2, we show the following result.

Lemma S.4.1. *Let g be a traveling wave of speed v with phenotypic threshold s . Then for all $x \in [L, 0]$ the following holds.*

- If $\gamma \leq \gamma_c$ then

$$A(x) = A^+(x) = \min(x + v, 0).$$

- If $\gamma > \gamma_c$, then

$$A(x) = \min(s - v, \max(x + v, d)) \quad \text{and} \quad A^+(x) = \min(0, \max(x + v, d)).$$

Proof. Let $x \in [L, 0]$ be the location of a genotype relative to the rightmost genotype at generation 1, that is, relative to v . Let $c \in [L + v, v]$ be the actual location of this genotype, so that $c = x + v$.

If $\gamma \leq \gamma_c$, then Theorem S.3.1 shows that $g' \in (-1, 1]$ (we can only have $g' = 1$ on the interval $[L, -(K - 1)v]$ when $2/\mu$ is an integer). Therefore, it is not hard to see that the maximum of $y \mapsto g(y) - |c - y|$ is unique for all $c \in [L + v, v]$, and it is attained at c for $c \in [L + v, 0]$, and at 0 for $c \in [0, v]$. With the change of variables $x = c - v$ we see that $A(x) = A^+(x) = \min(x + v, 0)$.

We now turn to the case $\gamma > \gamma_c$. We first take $c \in [s - v, v]$. We use Theorem S.3.1 again to determine where the maximum of the function $y \mapsto g(y) - |c - y|$ is attained. Using the slopes given by the theorem, in particular noting that $g' = -1$ on the interval $(s - v, 0)$, we find that the maximum is attained everywhere on the interval $[s - v, 0 \wedge c]$.

Similarly, using Theorem S.3.1 one can see that the maximum of the function $y \mapsto g(y) - |c - y|$ is attained at c , if $c \in [(L + v) \vee d, s - v]$, and it is attained at d , if $c \in [L + v, d]$.

With the change of variables $x = c - v$ and using the definitions of the functions A and A^+ , we obtain

$$A(x) = \begin{cases} s - v, & \text{if } x \in [s - 2v, 0] \\ x + v, & \text{if } x \in [L \vee (d - v), s - 2v] \\ d, & \text{if } x \in [L, d - v], \end{cases}$$

and

$$A^+(x) = \begin{cases} \min(x + v, 0), & \text{if } x \in [s - 2v, 0] \\ A(x), & \text{if } x \in [L, s - 2v]. \end{cases}$$

The two relations above imply the second part of the lemma. \square

Proof of Theorem S.1.2. Lemma S.4.1 implies $A(x) = A^+(x) = 0$ for all $x \in [-v, 0]$, if $\gamma \leq \gamma_c$; and also $A(x) = s - v$ and $A^+(x) = \min(x + v, 0)$ for all $x \in [s - 2v]$, if $\gamma > \gamma_c$.

Lemma S.4.1 also implies that for any $x \in [L, 0]$, both $A^j(x)$ and $(A^+)^j(x)$ increase by at least v until they reach 0 or $s - v$. Since $L < \infty$ and $v > 0$ in both regimes ($\gamma \leq \gamma_c$ and $\gamma > \gamma_c$), the statements of the theorem about $A^j(x)$ and $(A^+)^j(x)$ follow. \square

Remark that in the semi-pulled case, $\mu \mapsto v - s$ increases. This hints at the fact that it takes longer for ancestral lines to meet in the large disorder regime. This is a possible explanation for the non-monotonicity in Figure 1 in the main text.

S.4.2 Genealogical structure.

We are now interested in the genealogical tree generated by tracing backward in time k distinct ancestral lineages. Unfortunately, the genealogical structure is inherently stochastic, and random coalescence times can not be read from the hydrodynamic limit. Thus, we need to go back to the stochastic model and understand the fluctuations of the system.

Rather than analyzing the original model directly, we consider a fully integrable variation. As we will demonstrate, this integrable model retains many key properties, suggesting that both the original and modified versions belong to the same universality class and share an identical genealogical structure. Given that the ancestral structure of the integrable model is known [44], we can use a comparative approach to derive the ansatz for N_e presented in the main text (see equations (4.7) and (4.8)). The following paragraphs will elaborate on this.

The exponential model. We consider an extension of the exponential model of Brunet and Derrida [9]. It was first introduced in [13] by Cortines and Mallein, and further analysed in Schertzer and Wences [44].

As in the original model, at every generation, the population is made of N^γ individuals and evolves in two steps at every generation.

Reproduction. An individual with genetic value x produces an infinite number of offspring whose genotypes are distributed according to an independent exponential Poisson point process (PPP) with intensity measure $e^{-(y-x)}dy$. Note that the exponential PPP is shifted in such a way that the distribution is centered at x . In particular, there are only finitely many offspring to the right of x , and infinitely “unfit” children to its left.

Selection. After reproduction, infinitely many children are present. We then select the N^γ individuals using a sampling scheme interpolating between truncation selection and Gibbs sampling as follows. Let $\mu > 0$. Because the intensity measure vanishes exponentially fast at ∞ , it can be shown that children after reproduction can be ranked in decreasing order. We first select the N rightmost genotypes (truncation selection), and then sample N^γ individuals without replacement according to the sampling weights $e^{\mu x}$ (Gibbs sampling). When $\mu = \infty$, this amounts to selecting the N^γ rightmost individuals. For $\mu = 0$, N^γ individuals are selected uniformly at random from the N rightmost children. Thus, as in the previous model, the μ parameter also captures the level of noise in the selection scheme.

Universal traveling wave. The exponential model and our original model share the same phenomenology summarized in Table 2. For the sake of presentation, we will restrict ourself to the “shape” and speed of the traveling wave solution presented in the next table.

Table 2: Table to test captions and labels.

	Fully-pulled wave	Semi-pulled wave
	$\gamma < \gamma_c(\mu)$	$\gamma > \gamma_c(\mu)$
Stationary profile		
Speed	non-decreasing function of γ	non-increasing function of γ (flat in the exponential model)
Slope of g at the front	$\mu - 1$	-1 and then $\mu - 1$ after some $-\chi > 0$

In order to justify the previous results, let us consider an initial configuration of particles $(x_0^i)_{i=1}^{N^\gamma}$ with a limiting log profile g_0 . Formally, we assume the existence of a function g_0 valued in $\mathbb{R}_+ \cup \{-\infty\}$ such that for every $a < b$

$$\frac{\log(\#\{i : x_0^i \in (a \log(N), b \log(N))\})}{\log(N)} \rightarrow \max_{(a,b)} g_0 \quad \text{in probability.}$$

The key observation about the exponential model is that the superposition of shifted exponential PPP is again a shifted exponential PPP. More precisely, if the \mathcal{P}_i ’s are independent exponential PPP respective intensity $e^{-(x-x_0^i)}$ (describing the position of the offspring after the reproduction step), then

$$\sum_i \mathcal{P}_i = \mathcal{P} \quad \text{in law}$$

where \mathcal{P} is again a shifted exponential PPP with intensity $e^{-(y-X_{eq}^N)}$ with a shift

$$X_{eq} \equiv X_{eq}(x_0^i) := \log \left(\sum_{i=1}^{N^\gamma} e^{x_0^i} \right)$$

We emphasize that this simple but crucial observation by Brunet and Derrida [9] makes the model fully integrable. We now make use of this fact to compute the genotypic profile after one generation.

Reproduction profile. Let us first consider the individuals $(r_0^i)_{i=0}^\infty$ after reproduction. By the previous observation,

$$\begin{aligned} \frac{\log(\mathbb{E}(\#\{i : r_0^i \in X_{eq}^N + (a \log(N), b \log(N))\}))}{\log(N)} &= \frac{\int_{a \log(N)}^{b \log(N)} e^{-x} dx}{\log(N)} \\ &= \max_{(a,b) \in \mathbb{R}_-} (-x). \end{aligned} \quad (\text{S.4.1})$$

By a second moment argument, one can easily prove that the expectation can be removed inside the log and yields

$$\frac{\log(\#\{i : r_0^i \in X_{eq} + (a \log(N), b \log(N))\})}{\log(N)} \rightarrow \max_{(a,b)} R, \text{ where } R(x) := \pi(-x) \quad (\text{S.4.2})$$

where the convergence is meant in probability and the projector π has the effect of setting the population to 0 when the “expected stochastic exponent” in (S.4.1) takes negative values (as highlighted in the main text).

For any $a \in \mathbb{R}$, define the shift operator θ_a

$$\forall x > 0, \theta_a f(x) = f(x - a)$$

and

$$\hat{X}_{eq} = \frac{X_{eq}}{\log(N)}.$$

The previous result implies that the set of individuals after reproduction has a limiting log-profile given by $\theta_{\hat{X}_{eq}} R(x)$.

Truncation. We now consider the system of particles after only retaining the N rightmost individuals. This leads to a truncation profile given by $\theta_{\hat{X}_{eq}} T(x)$ where

$$T(x) = \begin{cases} -x & \text{if } -1 < x < 0 \\ -\infty & \text{otherwise.} \end{cases} \quad (\text{S.4.3})$$

In words, the log-profile after truncation is obtained by cutting the reproduction profile to the left of $(\theta_{\hat{X}_{eq}} R)^{-1}(1) = 1$, so that the $\asymp N$ rightmost particles remain.

Gibbs selection. Let $\mathcal{T} = (z_i^0)_{i=1}^N$ be the individuals present after the truncation step. We now select without replacement N^γ particles according to the sampling weights $e^{\mu z_0^i}$. Let $z \in \mathcal{T}$ an individual at position $u \log(N)$ ($u \in (-1, 0)$). For the sake of simplicity, let us first assume that individuals are sampled with replacement and let

$$p_N(u) := N^\gamma \times \frac{e^{\mu u \log(N)}}{\sum_{i=1}^N e^{\mu z_0^i}}.$$

be the expected number of times our focal individual is selected. From (S.4.3), an easy computation shows that

$$\frac{\log(\sum_{i=1}^N e^{\mu z_0^i})}{\log(N)} \approx 1 - \mu.$$

so that

$$\frac{\log(p_N(u))}{\log(N)} \approx \gamma - 1 + \mu(1 + u)$$

As a conclusion, if we sample with replacement then

- If $\gamma - 1 + \mu(1 + u) > 0$, the individual is sampled infinitely many times as $N \rightarrow \infty$.
- If $\gamma - 1 + \mu(1 + u) < 0$, the probability of sampling the individual goes to 0 and is $\asymp N^{\gamma-1+\mu(1+u)}$.

With a little bit of extra work, we can then deduce that if we now sample without replacement (as we should), then the following dichotomy holds

- If $\gamma - 1 + \mu(1 + u) > 0$ the probability of sampling the individual goes to 1.
- If $\gamma - 1 + \mu(1 + u) < 0$ the probability of sampling the individual is $\asymp N^{\gamma-1+\mu(1+u)}$.

We can then deduce that the log-profile of genotypes after one generation is $\theta_{\hat{X}_{eq}(x_0)} G$ where

$$G(x) = \begin{cases} \pi(-x + (\gamma - 1 + \mu(1 + x)))_- & \text{if } -1 < x < 0 \\ -\infty & \text{otherwise.} \end{cases}$$

To summarize the previous heuristics, one striking feature of the exponential model is that the wave reaches “stationarity” after only 1 generation and the only effect of the initial configuration is in the shift $\theta_{\hat{X}_{eq}(x_0)}$. It then follows that G is a traveling wave solution with a speed given by the limit of $\hat{X}_{eq}(x_0)$, where $(x_0^i)_{i=1}^{N^\gamma}$ is a configuration with a limiting log profile G .

As in our original model, we can now distinguish between two regimes from the explicit description of G . Define

$$\chi(\mu, \gamma) \equiv \chi := 1 - \frac{1 - \gamma}{\mu}$$

and define

$$\gamma_c(\mu) := 1 - \mu$$

so that $\chi > 0$ iff $\gamma > \gamma_c$.

Weak regime. $\gamma > \gamma_c$. Then G is obtained by concatenating continuously two linear functions with respective slopes -1 and $-(1 - \mu)$ at $-\chi$. That is

$$G(x) = \begin{cases} -x & \text{if } x \in (-\chi, 0) \\ \chi - (1 - \mu)(x - \chi) & \text{if } x \in (-1, -\chi) \\ -\infty & \text{otherwise.} \end{cases}$$

From the previous computations, we see that the slope at the tip is -1 and then $-(1 - \mu)$. The change of slope occurs at $-\chi$.

Let us now consider the speed of the wave and its monotonicity in γ . Recall that the speed is given by

$$\hat{X}_{eq}(x_0^N) = \frac{1}{\log(N)} \log\left(\sum_{i=0}^{N^\gamma} e^{\mu x_i^0}\right) \quad (\text{S.4.4})$$

where (x_0^i) has limiting log-profile G . The expression of G and a direct computation yields that the speed is given by

$$v \approx \frac{\log(\chi(\mu, \gamma))}{\log(N)} \rightarrow 0 \quad (\text{S.4.5})$$

so that in the semi-pulled regime, the wave is static in the natural scaling of the system (that is in $\log(N)$ units).

Strong regime ($\gamma < \gamma_c$). Define α through the relation

$$\alpha + (\gamma - 1 + \mu(1 - \alpha)) = 0 \iff \alpha = 1 - \frac{\gamma}{1 - \mu} \in (0, 1).$$

Then

$$G(x) = \begin{cases} -(1 - \mu)(x + \alpha) & \text{if } x \in (-1, -\alpha) \\ -\infty & \text{otherwise.} \end{cases}$$

and a direct computation from (S.4.4) shows that

$$v(\mu, \gamma) \approx -\alpha = \frac{\gamma}{1-\mu} - 1 > 0. \quad (\text{S.4.6})$$

It follows that v is now increasing in γ .

Finally, putting all the previous results together yields Table 2.

Genealogies. The exponential model preserves the properties of the original model summarized in Table 2. Those properties were derived (analogously to the original model) by looking at the limiting log-profile after one generation. Since all other properties listed in Table 1 (ancestry, selection etc.) follow from this analytical approach, it is not hard to extend the previous computations and show that actually all the properties listed in Table 1 also holds for the exponential model.

This hints at the fact that the two models fall in the same universality class, so that the same genealogical structure should emerge in the infinite population limit. Let us now recall one of the main results for the exponential model derived in [44]. See Theorem 2.7 in [44] for a more precise statement.

For a population of size N , let Π_k^N be the random genealogy obtained by sampling k individuals at a given time horizon and tracing their ancestral lineages backward in time. (Formally, this is encoded as an ultra-metric tree rooted at the most recent common ancestor of the sample, or as a coalescent process [41].) In [44], we proved that for a fixed value of $\mu \in (0, 1)$, then

1. If $\gamma < \gamma_c(\mu)$, Π_k^N converges to the (discrete) Poisson Dirichlet coalescent with parameter $(1-\mu, 0)$. See [44] for a definition. In particular, lineages coalesce in finite time and for $k = 2$, and the effective population size is given by

$$N_e \equiv \mathbb{E} [T_2^N] \approx \frac{1}{\mu} \quad (\text{S.4.7})$$

2. If $\gamma > \gamma_c(\mu)$, then the coalescence time between two lineages go to ∞ and we need to accelerate time by $\chi \log(N)$ in order to see an interesting picture emerging. After this proper time rescaling, the tree Π_k^N converges to the Bolthausen-Sznitman coalescent [41]. In particular, [44] proved that

$$N_e = \mathbb{E} [T_2^N] \approx \chi(\mu, \gamma) \log(N) \quad (\text{S.4.8})$$

This is the ansatz used in Section 4.2 for the model with phenotypic noise which is in good accordance with our numerical simulations. See Fig 3 in the main text.

S.5 Corrections to the limit theorems

The question of the deviation of finite size models from their deterministic approximations is of fundamental importance since those limits involve log transforms and change of scales in $\log(N)$. As expected, our numerical simulations show measurable errors from their infinite population prediction. See again Figure 3 in the main text.

Before explaining the origin of those deviations, we note that despite the fact that our hydrodynamic results only provide rough approximates on the precise values for the rate of adaptation and the effective population size (even at large N), our numerical simulations show that our limit theorems still capture the main qualitative behavior of the system. In particular, we can predict the existence of a phase transition between a strong and weak regime (change of monotonicity in the evolution speed $\gamma \rightarrow v(\beta, \gamma)$ and in the effective population size $\beta \rightarrow N_e(\mu, \gamma)$). Further, the critical value $\gamma_c(\mu)$ is well predicted by our limit theorems. See the bottom left pannel of Figure 3 in the main text.

Order of the corrections. Since the exponential model is fully integrable, it can inform us on the order of the finite-size population deviations from the limit theorems. In [44], we derived precise asymptotics for the rate of adaptation which extend the heuristics from the previous section (see (S.4.5, S.4.6)). We proved that

1. for $\gamma < \gamma_c(\mu)$, then

$$v_N \approx -(1 - \frac{\gamma}{1 - \mu}) + \frac{\mathbb{E}[\log(Y_\mu)]}{\log(N)} + o(\frac{1}{\log(N)}) \quad (\text{S.5.1})$$

where Y_μ is a $(1 - \mu)$ positive stable random variable whose Laplace transform is given by

$$\mathbb{E}[e^{-\lambda Y_\mu}] = \exp(-\Gamma(\mu)\lambda^{1-\alpha}) \quad (\text{S.5.2})$$

2. For $\gamma > \gamma_c(\mu)$, then

$$v_N \approx \frac{\log(\chi(\mu, \gamma) \log(N))}{\log(N)} + o(\frac{1}{\log(N)})$$

We then have two kinds of correction depending on the regime. Either $\asymp 1/\log(N)$ when $\gamma < \gamma_c$, or $\log(\log(\chi(\mu, \gamma)/\log(N)))$ when $\gamma > \gamma_c$. Note that both corrections explode when $\gamma \rightarrow \gamma_c(\mu)$ which indicates that the $o(1)$ correction should explode at the critical point. A different theory is then needed to grasp the behavior of the system at criticality (or near criticality).

In addition, we plotted the estimation of the speed for different values of K in the exponential model. See the top right pannel of Figure 3 in the main text. We see that the higher order correction terms make the convergence to the theoretical rescaled speed extremely slow. This is particularly true in the semi-pushed regime ($\gamma > \gamma_c(\mu)$) because of the correction in $\log(\chi \log(N))/\log(N)$. A similar pattern is observed in our original model. Extending our methods to quantify the error terms (as in the exponential model) remains an important but presumably difficult challenge.

S.6 Sexual reproduction

We consider a sexual version of the asexual model exposed in the main text. As before, at every generation n , the population consists of N^γ individuals. The population evolves from $n - 1$ to n into two successive steps.

Step 1. Reproduction. We generate N offspring. Each offspring has two parents (x_1, x_2) chosen uniformly at random from generation $n - 1$. The genotype and phenotype of is individual is obtained by adding noise to the mean parental genotype values, that is

$$\text{genotype} = \frac{1}{2}(x_1 + x_2) + X, \quad \text{phenotype} = \frac{1}{2}(x_1 + x_2) + X + Y,$$

where X and Y have respective distribution f_X and f_Y

$$f_X(x) = \frac{1}{2} \exp(-|x|), \quad f_Y(x) = \frac{\mu}{2} \exp(-\mu|x|),$$

for a fixed value of $\mu > 0$ which captures the inverse of the phenotypic noise.

Step 2. Selection. As for the asexual case, the population at generation n is obtained by selecting the N^γ genotypes with the N^γ rightmost phenotypes.

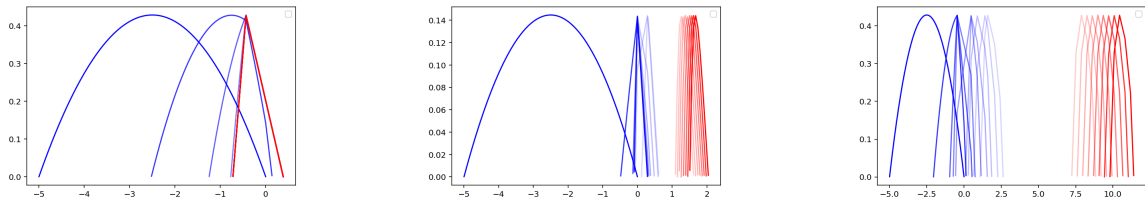


Figure 5: Fitness wave for the sexual model. In blue : generation 0 to 8. In red: generation 16 to 24.

From left to right: static regime ($\mu = .48, \gamma = .43$); close to static ($\mu = .51, \gamma = .14$); moving ($\mu = .61, \gamma = .61$)

Log-profiles. As in the asexual case, we can derive a recursive equation for the limiting stochastic exponents. At generation $n - 1$, we think of $N^{g_{n-1}(x)}dx$ as the number of particles in $dx \log(N)$. We

claim that if g_0 is concave on its support (that is the set of points where $g_0(x) \neq -\infty$), then for every $n \geq 0$

$$g_n(x) = \pi \left[\sup_{y \in \mathbb{R}} (1 - 2\gamma + 2g_{n-1}(y) - |x - y| - \mu(s_n - x)_+) \right], \quad (\text{S.6.1})$$

where s_n satisfies $\sup g_n = \gamma$,

In order to justify the formula, we note that the average number of offspring with parents in (dx_1, dx_2) is approximately

$$\frac{N^{g_{n-1}(x_1)} N^{g_{n-1}(x_2)}}{N^{2\gamma}} N dx_1 dx_2.$$

Along the lines of the asexual case, this yields

$$g_n(x) = \pi \left[\sup_{y_1, y_2 \in \mathbb{R}} \left(1 - 2\gamma + g_{n-1}(y_1) + g_{n-1}(y_2) - \left| x - \frac{y_1 + y_2}{2} \right| - \mu(s_n - x)_+ \right) \right], \quad (\text{S.6.2})$$

where s_n satisfies $\sup g_n = \gamma$,

Now, assume that g_{n-1} is concave on its support. Then

$$\forall y_1, y_2 \in \text{Supp}(g_{n-1}), \quad g_{n-1}(y_1) + g_{n-1}(y_2) \leq 2g_{n-1}\left(\frac{y_1 + y_2}{2}\right).$$

so that (S.6.1) must hold. Since g_0 is assumed to be concave on its support, it remains to show that concavity is preserved by the dynamics. This easily follows from Lemma S.2.1.